# MONITORING DEFORMATION OF BRIDGES WITH INSAR

## Proof of Concept

## Technical Report

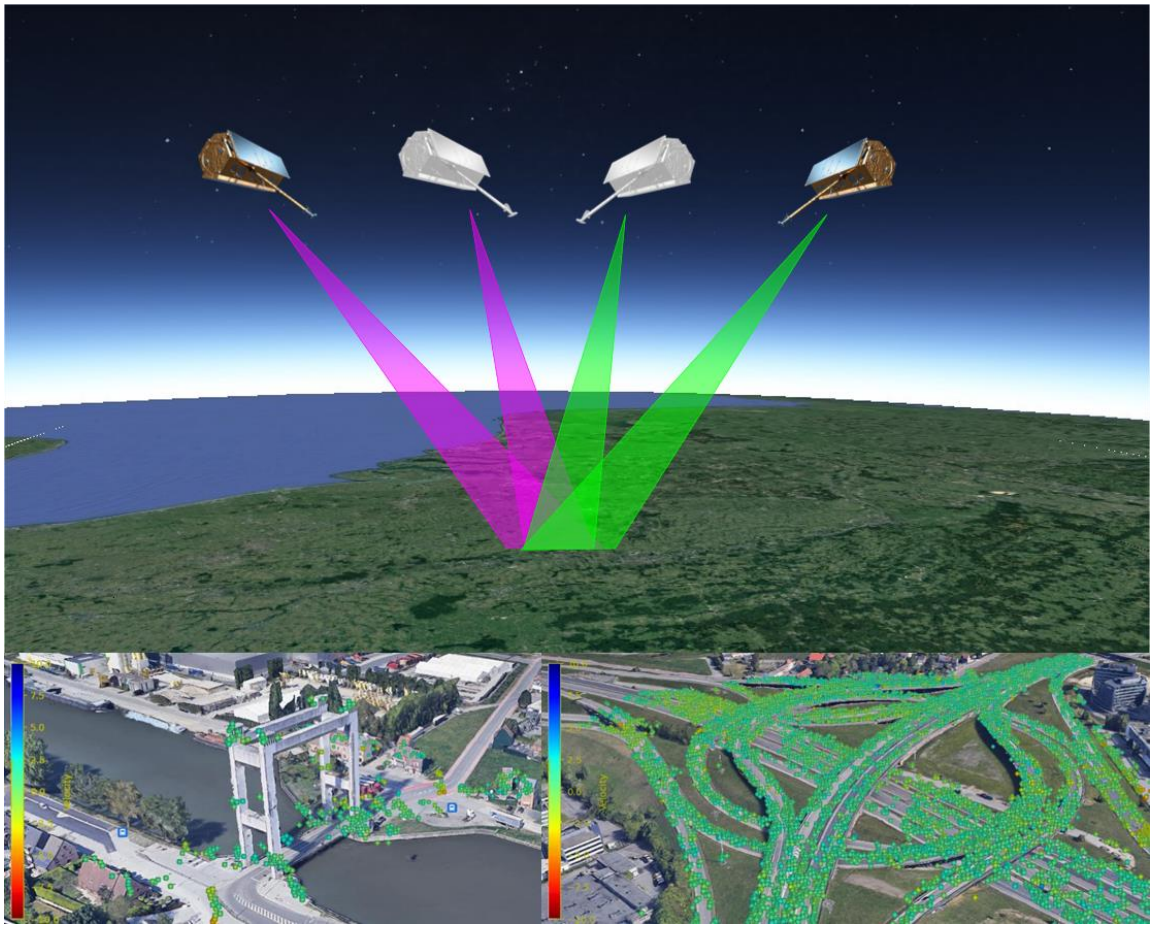

Document: CMM-PRO-21-050_POC_Technical Report

Issue: 1.1

Date: 31/12/2021

***NOT CLASSIFIED***
***This document discloses subject matter in which e-GEOS has proprietary rights. Recipient of the document shall not duplicate, use or disclose in whole or in part, information contained herein except for or on behalf of e-GEOS to fulfil the purpose for which the document was delivered to him.***

| Document: CMM-PRO-21-050_POC_Technical Report | | | | |
|---|---|---|---|---|
| **Version** | **Date** | **Authors** | **Verified** | **Reason of the modification** |
| 1.1 | 31/12/2021 | C. Frascella<br>S. Falco<br>N. Belcecchi | F. Minati<br>S. Scancella<br>A.Priolo | Revision of First Issue with the following main updates, provided after the final meeting:<br>• Inclusion (§9) of the technical note delivered on 24th December 2021 with analysis on the lack of MPs over some bridges<br>• Revision of §10 with documentation of the compliances with the Tender requirements<br>• General revision of document format (mainly using A4 for the Document, and A3 only for the final ANNEX). |

*NOT CLASSIFIED*
*This document discloses subject matter in which e-GEOS has proprietary rights. Recipient of the document shall not duplicate, use or disclose in whole or in part, information contained herein except for or on behalf of e-GEOS to fulfil the purpose for which the document was delivered to him.*

# Table of Contents



*NOT CLASSIFIED*
*This document discloses subject matter in which e-GEOS has proprietary rights. Recipient of the document shall not duplicate, use or disclose in whole or in part, information contained herein except for or on behalf of e-GEOS to fulfil the purpose for which the document was delivered to him.*

# GLOSSARY AND ACRONYMS

**AOI** Area of interest

**A-DInSAR**
A-DInSAR is an acronym for “Advanced Differential Interferometric Synthetic Aperture Radar”. This term groups several processing techniques based on multi-temporal stacks (see “Stack”) of satellite SAR images.

**DS** Distributed Scatterers

**LOS** Line of sight of the satellite (measured along the sensor-target line).

**GIS** Geographic Information System

**Orbital geometry**
Satellites equipped with SAR sensors fly around the Earth along approximately N-S orbits. Therefore, satellites fly over the same area both during the ascending (South to North) and descending (North to South) orbits. Due to the inclination of the line of sight (LOS) with respect to the nadir, the satellite is able to look the same area from two different points of view, during the data acquisition. Most of the satellites use a right-looking configuration (they look to the right), so in ascending geometry the images are acquired from the West (LOS directed to the East), while in descending geometry images are acquired from East (LOS directed to the West).

**PS** Persistent Scatterers

**PSP-IFSAR** Persistent Scatterers Pair SAR Inferferometry

**RADAR**
RADAR is an acronym for “RAdio Detection And Ranging”: it is an object-detection system that uses electromagnetic waves to define the range, angle, or velocity of objects. A RADAR system for SAR applications consists of a transmitter emitting a microwave signal and of a receiving antenna that acquires the backscattered signal. The system is based on the measure of the Time of Flight (TOF), namely the time required by the signal to travel from the sensor to the target.

**S1** Sentinel-1

**SAR**
SAR is an acronym for “Synthetic Aperture Radar”. It is a specific kind of RADAR which takes advantage of its movement along its default trajectory (e.g. satellite orbit) to synthetize a large antenna, allowing to get better ground resolution.

**Stack**
Multi-temporal dataset of SAR images acquired with the same features (resolution, orbit geometry, incidence angle, etc.) on the same area in a given time interval. It represents the input raw data for analysis with the A-DInSAR approach.

**TSX** TerraSAR-X

*NOT CLASSIFIED*
*This document discloses subject matter in which e-GEOS has proprietary rights. Recipient of the document shall not duplicate, use or disclose in whole or in part, information contained herein except for or on behalf of e-GEOS to fulfil the purpose for which the document was delivered to him.*

# 1. Introduction

This technical report contains the results of the Proof of Concept (PoC) for the Phase 2 of the Competition procedure with negotiation, specifications n. 49616 GEO_2021-01, emitted by the Department of Mobility and Public Works of the Flemish Government. The activity is carried out by the consortium composed by e-GEOS S.p.a. as prime contractor and NHAZCA S.r.l. as partner contractor, temporally grouped specifically to submit jointly the reply to the Competition. Together, e-GEOS and NHAZCA describe a team with outstanding experience in the field of Earth Observation services, serving and consulting public institutions and large corporate entities in many Geo Information System activities and specifically on InSAR analysis, providing a first-class quality result.

The aim of the POC is to identify, map and characterize infrastructures deformation processes affecting the area, with the scope to assess the added value of InSAR analysis technique to monitor the deformations of bridges, to specifically evaluate the percentage of bridges that can be monitored with this method, and to clarify the need of purchasing high resolution radar images.

The A-DInSAR analyses have been performed using the available archive SAR images collected by:

- the Sentinel-1 satellite constellation (European Space Agency), acquired in double geometry (ascending and descending) in the period February 2015 - August 2021. The ascending and descending datasets are constituted by 325 and 334 SAR images with ground resolution of 4m × 14m, respectively;
- the TerraSAR-X satellite, acquired in descending acquisition geometry in the period June 2014 and March 2016. The dataset is constituted by 53 high-resolution SAR images, with ground resolution of 3m x 3m.

This report presents: the context of the AOI (Figure 1, Table 1), located in Brussels; the performed activities carried out in the execution of this POC. In particular, a focus on the type of utilized data, a description of the analyses and an overview on the adopted algorithms is going to be presented; in the end, the results will be explained in detail, providing a summary of the fulfillment of the minimum and additional tender procedure requirements.

The results of the A-DInSAR analysis will be also provided in shapefile format and through AWARE Platform (https://aware.egeos-services.it) the web portal specifically designed for assets monitoring, for an interactive visualization of the data. A separate document will be provided with the end-user manual of AWARE platform.

An Appendix to the report is enclosed, in order to provide an introduction to the SAR systems and data, to the differential SAR interferometric technique and to the SAR satellite constellation.

*NOT CLASSIFIED*
*This document discloses subject matter in which e-GEOS has proprietary rights. Recipient of the document shall not duplicate, use or disclose in whole or in part, information contained herein except for or on behalf of e-GEOS to fulfil the purpose for which the document was delivered to him.*

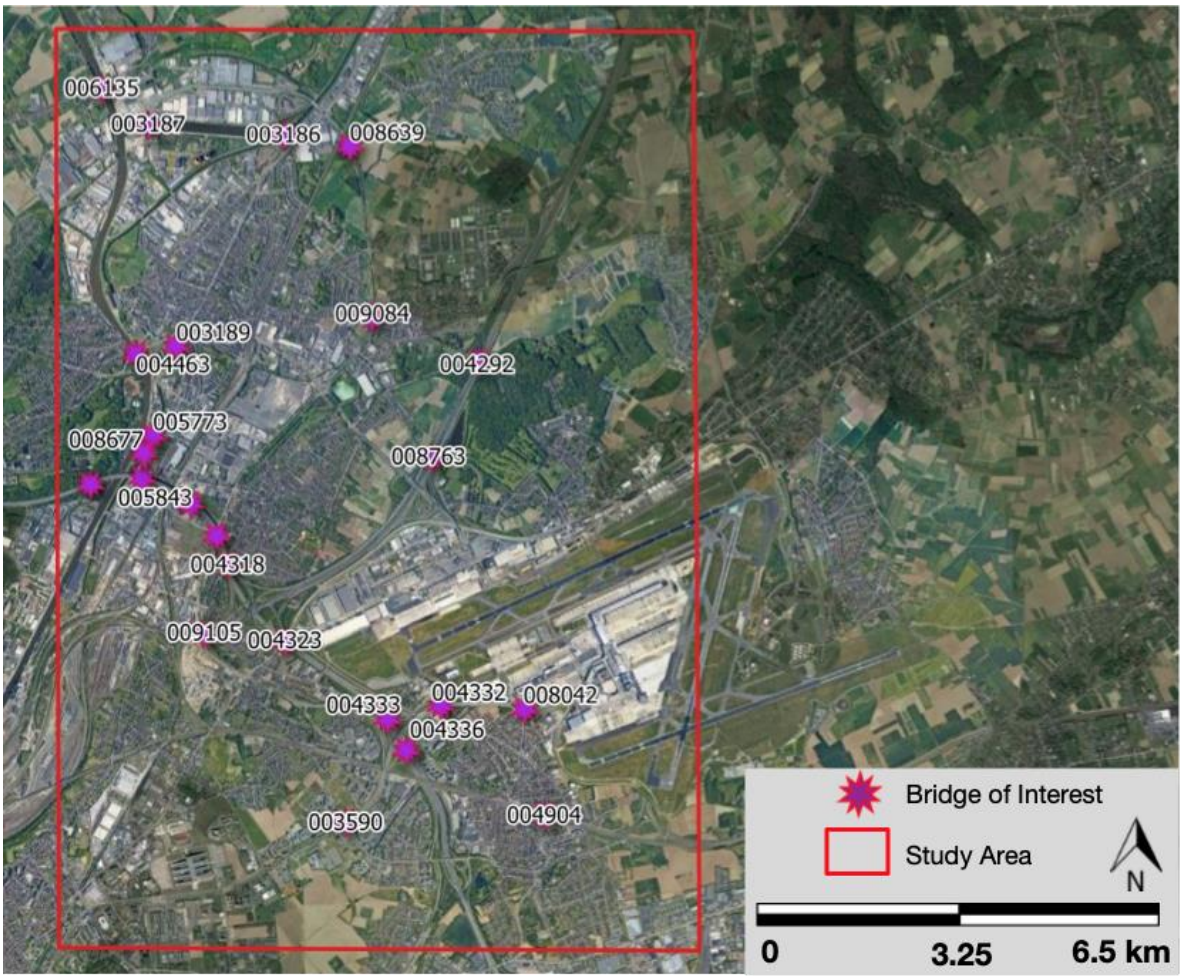


**Figure 1: Area of interest of the PoC and location of the bridges of interest provided by the client**

| Object Nummer | Name |
|---|---|
| 3186 | Havendoklaanbrug |
| 5773 | Sluisstraatbrug |
| 6135 | Verbrande Brug |
| 4463 | Hefbrug Vilvoordebrug Vuurkruisenlaan-Rubensstraat Europabrug |
| 4292 | Brug B14 |
| 8042 | Viaduct in A201 over N262 |
| 4333 | Brug R18 |
| 4336 | Brug R21 |
| 5843 | Viaduct R7 Deel B |
| 5844 | Viaduct R7 Deel C |
| 5845 | Viaduct R7 Deel D |
| 4317 | Viaduct R7 Deel A |
| 3187 | Willemsbrug |

*NOT CLASSIFIED*
*This document discloses subject matter in which e-GEOS has proprietary rights. Recipient of the document shall not duplicate, use or disclose in whole or in part, information contained herein except for or on behalf of e-GEOS to fulfil the purpose for which the document was delivered to him.*

| | |
|---|---|
| 8639 | Fiets- en voetbrug Schoewever Woluwelaan |
| 9084 | Voet- en fietsbrug Kleine Steenstraat |
| 8763 | Fietsbrug over E19 + Noordelijke spoorontsluiting luchthaven |
| 8677 | Brug over de Zenne met verbindingsweg naar sluis |
| 9105 | Spoorwegbrug in Spoorlijn 25N over R22 |
| 3189 | Tuchthuisbrug |
| 4318 | Brug R8 P. Schoonstraat Oudstrijdersstraat |
| 3590 | Brug 1 over de J. F. Kennedylaan Grensstraat |
| 4323 | Brug R15 |
| 4904 | Brug in N262 Parklaan over spoorweg |
| 4332 | Brug D5 Steenweg op Zaventem |

**Table 1: List of the bridges on the present PoC**

## 2. Brussels AOI Context

In order to contextualize the A-DInSAR results in the geomorphological framework of the site and to integrate the information obtained in the analysis of the deformation processes over the study area, a study of the literature has been carried out with particular attention to InSAR and geological/geomorphological previous works (Declercq et al., 2021, 2017, Choopani et al., 2021). In particular, Declercq et al., 2021 and 2017, used SAR Interferometry with older datasets with respect to the one used in the present document (e.g., ERS, ENVISAT, starting since 1992 up to 2010) to investigate the historical ground deformation of Brussels and surrounding areas. All of these works are aligned with the presence of a regional uplift affecting Brussels with variable rates among the several satellite constellations, from 1 to 10 mm/yr (Figure 2). Those authors stated that the regional uplift can be ascribed to the strong exploitation of the aquifers for water supply occurred in the 19$^{th}$ and beginning of the 20$^{th}$ centuries and, by InSAR, satellites are now measuring the effect of the recharge on the aquifers. The aquifers exploitation occurred over several superposed Quaternary to Cambro-Silurian aquifers, affecting in particular the along the Senne river alluvial deposits (in the NE-SW direction). The authors derived that the area affected by the strongest positive ground deformations matches perfectly to the zone of water catchments and groundwater pumping since the industrialization of Brussels and now satellites are measuring the combined effect of the recharge of the Cretaceous aquifer and the phreatic aquifer of the Senne river.

*NOT CLASSIFIED*
*This document discloses subject matter in which e-GEOS has proprietary rights. Recipient of the document shall not duplicate, use or disclose in whole or in part, information contained herein except for or on behalf of e-GEOS to fulfil the purpose for which the document was delivered to him.*

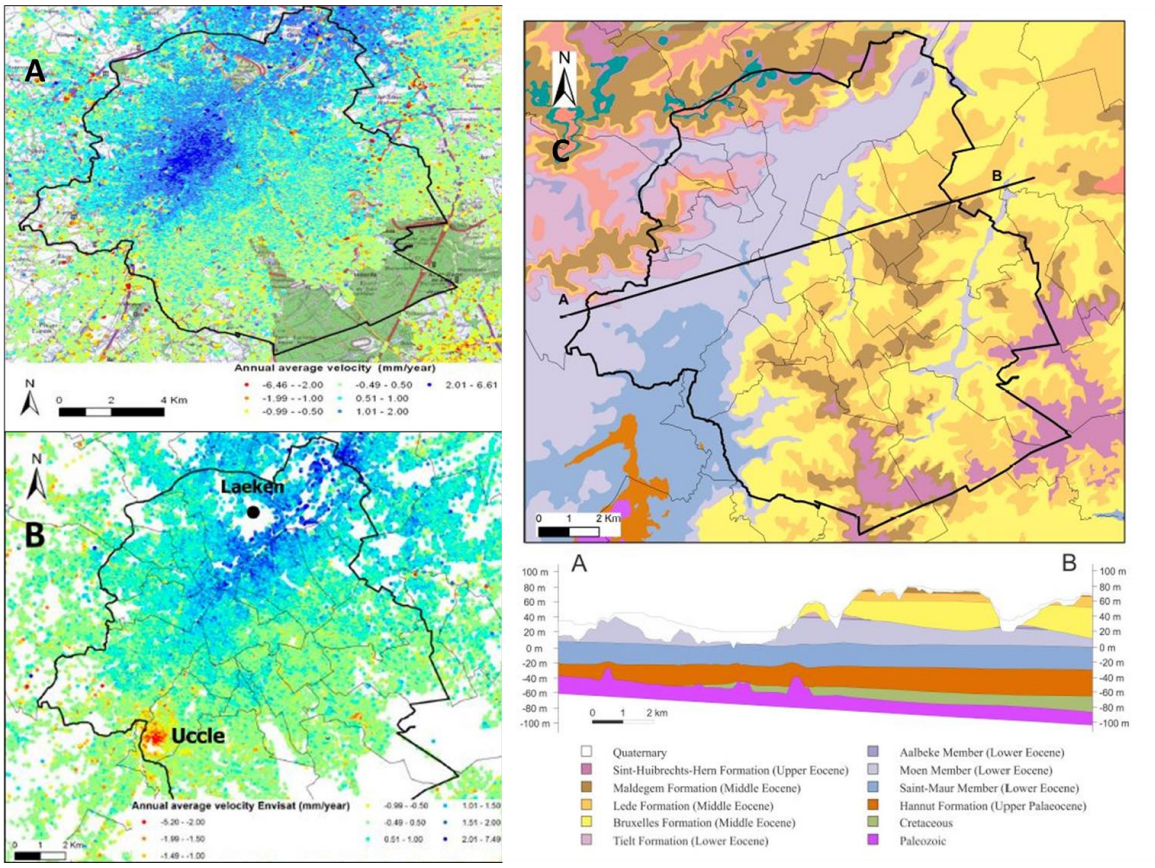


**Figure 2: Average annual velocities of measurement points with ERS (A) 1992-2006; ENVISAT (B) 2003-2010; In C, geological map and cross section profile through the Brussel region. Modified from Declercq et al., 2017.**

## 3. Performed activities

In what follows, the performed activities are described. Specifically, the following work packages have been carried out:

- Selection and acquisition of the datasets and auxiliary data:
  - Sentinel-1, by European Space Agency archives (Sect. 4)
  - TerraSAR-X, Deutsches Zentrum für Luft- und Raumfahrt, provided by the Client (Sect. 4)
  - EuDEM an European Environment Agency (EEA) digital surface model (25m resolution), used for interferograms computations and geocoding of the measurement points.

*NOT CLASSIFIED*
*This document discloses subject matter in which e-GEOS has proprietary rights. Recipient of the document shall not duplicate, use or disclose in whole or in part, information contained herein except for or on behalf of e-GEOS to fulfil the purpose for which the document was delivered to him.*

- A-DInSAR processing of satellite SAR images by proprietary PSI processing chains. In particular, e-GEOS developed and patented the PSP-IFSAR processing chain, and NHAZCA makes use of proprietary processing chain and tools developed in Matlab© and Python languages (Sect. 5)

- Presentation of the results achieved by A-DInSAR (Sect. 7)

- Post-processing and validation, to support the asset management and the performance analyses of the bridges starting from the results derived from satellite SAR Interferometry (Sect. 8 and Annex 1).

# 4. Type and characteristics of satellite and auxiliary data used

For this study, three datasets (interferometric stacks) of satellite SAR images including the study area have been employed:

- **325 Sentinel-1 SAR scenes** in **ascending** orbital geometry covering a period of about 6.5 years (**February 2015 – July 2021**), acquired by the ESA archives (Figure 3, Figure 4, Table 2);
- **334 Sentinel-1 SAR scenes** in **descending** orbital geometry covering a period of about 6.5 years (**March 2015 – August 2021**), acquired by the ESA archives (Figure 3, Figure 4, Table 3);
- **53 SAR TerraSAR-X scenes** in **descending** orbital geometry covering a period of about 1.5 years (**June 2014 – March 2016**), provided by the Client (Figure 3, Figure 4, Table 4).

The footprints of the analyzed images are reported in Figure 3, while the acquisition calendars of the analyzed SAR images are reported in Table 2, Table 3 and Table 4.

*NOT CLASSIFIED*
*This document discloses subject matter in which e-GEOS has proprietary rights. Recipient of the document shall not duplicate, use or disclose in whole or in part, information contained herein except for or on behalf of e-GEOS to fulfil the purpose for which the document was delivered to him.*

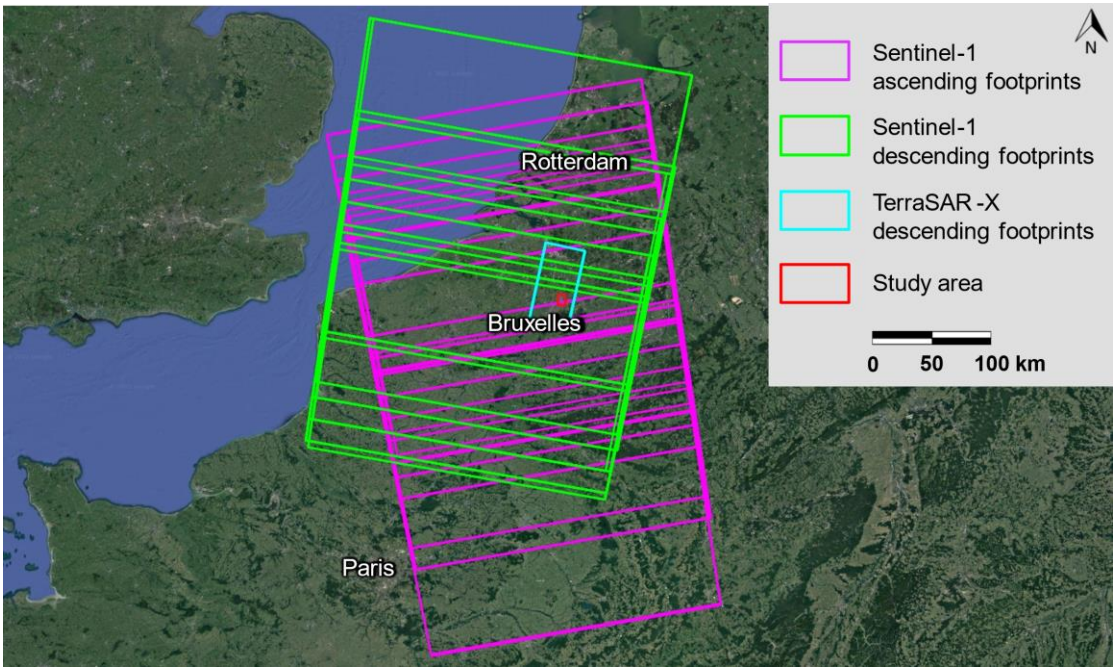


**Figure 3: identification of the study area on satellite optical image and footprints of the analyzed Sentinel-1 (ascending and descending) and TerraSAR-X (descending) datasets.**

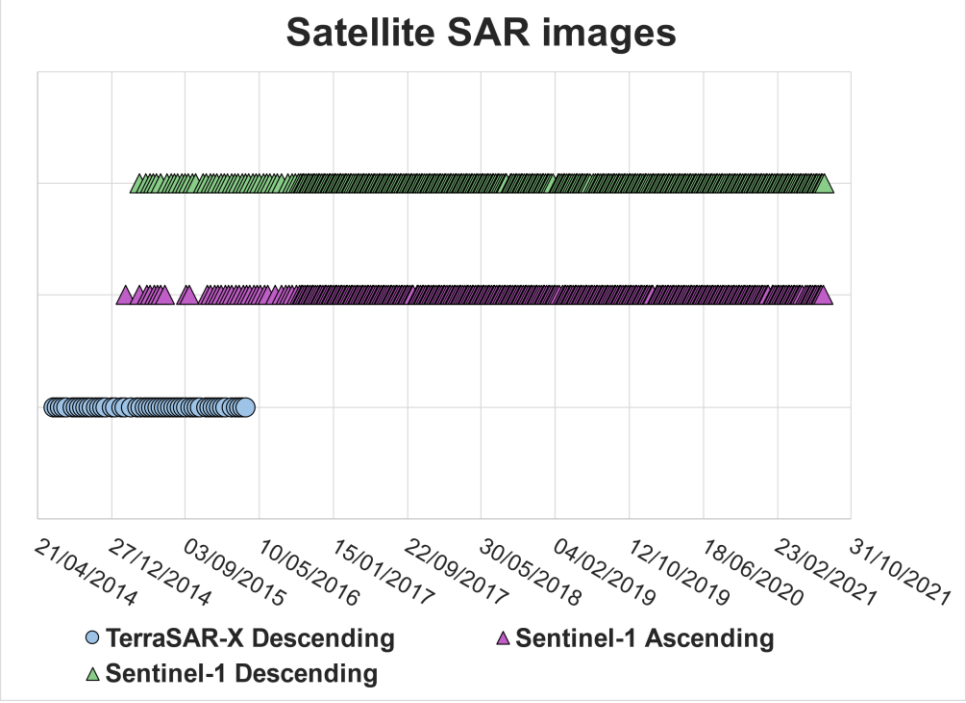


**Figure 4: temporal distribution of the analyzed SAR images.**

*NOT CLASSIFIED*
*This document discloses subject matter in which e-GEOS has proprietary rights. Recipient of the document shall not duplicate, use or disclose in whole or in part, information contained herein except for or on behalf of e-GEOS to fulfil the purpose for which the document was delivered to him.*

| Sentinel-1 Ascending | | | | | | | | | | | | | |
|---|---|---|---|---|---|---|---|---|---|---|---|---|---|
| 1 | 13/02/2015 | 51 | 28/12/2016 | 101 | 30/10/2017 | 151 | 26/08/2018 | 201 | 28/06/2019 | 251 | 29/04/2020 | 301 | 01/03/2021 |
| 2 | 02/04/2015 | 52 | 03/01/2017 | 102 | 05/11/2017 | 152 | 01/09/2018 | 202 | 04/07/2019 | 252 | 05/05/2020 | 302 | 07/03/2021 |
| 3 | 26/04/2015 | 53 | 09/01/2017 | 103 | 11/11/2017 | 153 | 07/09/2018 | 203 | 10/07/2019 | 253 | 11/05/2020 | 303 | 13/03/2021 |
| 4 | 08/05/2015 | 54 | 15/01/2017 | 104 | 17/11/2017 | 154 | 13/09/2018 | 204 | 16/07/2019 | 254 | 17/05/2020 | 304 | 19/03/2021 |
| 5 | 20/05/2015 | 55 | 21/01/2017 | 105 | 23/11/2017 | 155 | 19/09/2018 | 205 | 22/07/2019 | 255 | 23/05/2020 | 305 | 25/03/2021 |
| 6 | 01/06/2015 | 56 | 27/01/2017 | 106 | 29/11/2017 | 156 | 25/09/2018 | 206 | 28/07/2019 | 256 | 29/05/2020 | 306 | 31/03/2021 |
| 7 | 13/06/2015 | 57 | 02/02/2017 | 107 | 05/12/2017 | 157 | 01/10/2018 | 207 | 03/08/2019 | 257 | 04/06/2020 | 307 | 06/04/2021 |
| 8 | 25/06/2015 | 58 | 08/02/2017 | 108 | 11/12/2017 | 158 | 07/10/2018 | 208 | 09/08/2019 | 258 | 10/06/2020 | 308 | 12/04/2021 |
| 9 | 05/09/2015 | 59 | 14/02/2017 | 109 | 17/12/2017 | 159 | 13/10/2018 | 209 | 15/08/2019 | 259 | 16/06/2020 | 309 | 18/04/2021 |
| 10 | 17/09/2015 | 60 | 20/02/2017 | 110 | 23/12/2017 | 160 | 19/10/2018 | 210 | 21/08/2019 | 260 | 22/06/2020 | 310 | 24/04/2021 |
| 11 | 16/11/2015 | 61 | 26/02/2017 | 111 | 29/12/2017 | 161 | 25/10/2018 | 211 | 27/08/2019 | 261 | 28/06/2020 | 311 | 30/04/2021 |
| 12 | 28/11/2015 | 62 | 04/03/2017 | 112 | 04/01/2018 | 162 | 31/10/2018 | 212 | 02/09/2019 | 262 | 04/07/2020 | 312 | 06/05/2021 |
| 13 | 10/12/2015 | 63 | 10/03/2017 | 113 | 10/01/2018 | 163 | 06/11/2018 | 213 | 08/09/2019 | 263 | 10/07/2020 | 313 | 12/05/2021 |
| 14 | 22/12/2015 | 64 | 16/03/2017 | 114 | 16/01/2018 | 164 | 12/11/2018 | 214 | 14/09/2019 | 264 | 16/07/2020 | 314 | 18/05/2021 |
| 15 | 03/01/2016 | 65 | 22/03/2017 | 115 | 22/01/2018 | 165 | 18/11/2018 | 215 | 20/09/2019 | 265 | 22/07/2020 | 315 | 30/05/2021 |
| 16 | 15/01/2016 | 66 | 28/03/2017 | 116 | 28/01/2018 | 166 | 24/11/2018 | 216 | 26/09/2019 | 266 | 28/07/2020 | 316 | 05/06/2021 |
| 17 | 27/01/2016 | 67 | 03/04/2017 | 117 | 03/02/2018 | 167 | 30/11/2018 | 217 | 02/10/2019 | 267 | 03/08/2020 | 317 | 11/06/2021 |
| 18 | 08/02/2016 | 68 | 09/04/2017 | 118 | 09/02/2018 | 168 | 06/12/2018 | 218 | 08/10/2019 | 268 | 09/08/2020 | 318 | 17/06/2021 |
| 19 | 20/02/2016 | 69 | 15/04/2017 | 119 | 15/02/2018 | 169 | 12/12/2018 | 219 | 14/10/2019 | 269 | 15/08/2020 | 319 | 23/06/2021 |
| 20 | 03/03/2016 | 70 | 21/04/2017 | 120 | 21/02/2018 | 170 | 18/12/2018 | 220 | 20/10/2019 | 270 | 21/08/2020 | 320 | 29/06/2021 |
| 21 | 15/03/2016 | 71 | 27/04/2017 | 121 | 27/02/2018 | 171 | 24/12/2018 | 221 | 26/10/2019 | 271 | 27/08/2020 | 321 | 05/07/2021 |
| 22 | 27/03/2016 | 72 | 03/05/2017 | 122 | 05/03/2018 | 172 | 30/12/2018 | 222 | 01/11/2019 | 272 | 02/09/2020 | 322 | 11/07/2021 |
| 23 | 08/04/2016 | 73 | 09/05/2017 | 123 | 11/03/2018 | 173 | 05/01/2019 | 223 | 07/11/2019 | 273 | 08/09/2020 | 323 | 17/07/2021 |
| 24 | 20/04/2016 | 74 | 15/05/2017 | 124 | 17/03/2018 | 174 | 11/01/2019 | 224 | 13/11/2019 | 274 | 14/09/2020 | 324 | 23/07/2021 |
| 25 | 02/05/2016 | 75 | 21/05/2017 | 125 | 23/03/2018 | 175 | 17/01/2019 | 225 | 19/11/2019 | 275 | 20/09/2020 | 325 | 29/07/2021 |
| 26 | 14/05/2016 | 76 | 27/05/2017 | 126 | 29/03/2018 | 176 | 23/01/2019 | 226 | 25/11/2019 | 276 | 26/09/2020 | | |
| 27 | 26/05/2016 | 77 | 02/06/2017 | 127 | 04/04/2018 | 177 | 29/01/2019 | 227 | 01/12/2019 | 277 | 02/10/2020 | | |
| 28 | 07/06/2016 | 78 | 08/06/2017 | 128 | 10/04/2018 | 178 | 04/02/2019 | 228 | 07/12/2019 | 278 | 08/10/2020 | | |
| 29 | 01/07/2016 | 79 | 14/06/2017 | 129 | 16/04/2018 | 179 | 10/02/2019 | 229 | 13/12/2019 | 279 | 14/10/2020 | | |
| 30 | 25/07/2016 | 80 | 20/06/2017 | 130 | 22/04/2018 | 180 | 16/02/2019 | 230 | 19/12/2019 | 280 | 20/10/2020 | | |
| 31 | 06/08/2016 | 81 | 26/06/2017 | 131 | 28/04/2018 | 181 | 28/02/2019 | 231 | 25/12/2019 | 281 | 26/10/2020 | | |
| 32 | 18/08/2016 | 82 | 02/07/2017 | 132 | 04/05/2018 | 182 | 06/03/2019 | 232 | 31/12/2019 | 282 | 01/11/2020 | | |
| 33 | 30/08/2016 | 83 | 08/07/2017 | 133 | 10/05/2018 | 183 | 12/03/2019 | 233 | 12/01/2020 | 283 | 07/11/2020 | | |
| 34 | 11/09/2016 | 84 | 14/07/2017 | 134 | 16/05/2018 | 184 | 18/03/2019 | 234 | 18/01/2020 | 284 | 13/11/2020 | | |
| 35 | 23/09/2016 | 85 | 20/07/2017 | 135 | 22/05/2018 | 185 | 24/03/2019 | 235 | 24/01/2020 | 285 | 19/11/2020 | | |
| 36 | 29/09/2016 | 86 | 26/07/2017 | 136 | 28/05/2018 | 186 | 30/03/2019 | 236 | 30/01/2020 | 286 | 25/11/2020 | | |
| 37 | 05/10/2016 | 87 | 01/08/2017 | 137 | 03/06/2018 | 187 | 05/04/2019 | 237 | 05/02/2020 | 287 | 01/12/2020 | | |
| 38 | 11/10/2016 | 88 | 07/08/2017 | 138 | 09/06/2018 | 188 | 11/04/2019 | 238 | 11/02/2020 | 288 | 07/12/2020 | | |
| 39 | 17/10/2016 | 89 | 13/08/2017 | 139 | 15/06/2018 | 189 | 17/04/2019 | 239 | 17/02/2020 | 289 | 13/12/2020 | | |
| 40 | 23/10/2016 | 90 | 19/08/2017 | 140 | 21/06/2018 | 190 | 23/04/2019 | 240 | 23/02/2020 | 290 | 19/12/2020 | | |
| 41 | 29/10/2016 | 91 | 25/08/2017 | 141 | 27/06/2018 | 191 | 29/04/2019 | 241 | 29/02/2020 | 291 | 25/12/2020 | | |
| 42 | 04/11/2016 | 92 | 31/08/2017 | 142 | 03/07/2018 | 192 | 05/05/2019 | 242 | 06/03/2020 | 292 | 31/12/2020 | | |
| 43 | 10/11/2016 | 93 | 06/09/2017 | 143 | 09/07/2018 | 193 | 11/05/2019 | 243 | 12/03/2020 | 293 | 06/01/2021 | | |
| 44 | 16/11/2016 | 94 | 12/09/2017 | 144 | 15/07/2018 | 194 | 17/05/2019 | 244 | 18/03/2020 | 294 | 12/01/2021 | | |
| 45 | 22/11/2016 | 95 | 18/09/2017 | 145 | 21/07/2018 | 195 | 23/05/2019 | 245 | 24/03/2020 | 295 | 18/01/2021 | | |
| 46 | 28/11/2016 | 96 | 24/09/2017 | 146 | 27/07/2018 | 196 | 29/05/2019 | 246 | 30/03/2020 | 296 | 24/01/2021 | | |
| 47 | 04/12/2016 | 97 | 30/09/2017 | 147 | 02/08/2018 | 197 | 04/06/2019 | 247 | 05/04/2020 | 297 | 05/02/2021 | | |
| 48 | 10/12/2016 | 98 | 06/10/2017 | 148 | 08/08/2018 | 198 | 10/06/2019 | 248 | 11/04/2020 | 298 | 11/02/2021 | | |
| 49 | 16/12/2016 | 99 | 12/10/2017 | 149 | 14/08/2018 | 199 | 16/06/2019 | 249 | 17/04/2020 | 299 | 17/02/2021 | | |
| 50 | 22/12/2016 | 100 | 24/10/2017 | 150 | 20/08/2018 | 200 | 22/06/2019 | 250 | 23/04/2020 | 300 | 23/02/2021 | | |

**Table 2: acquisition dates (dd/mm/yyyy) of the analyzed SAR images – Sentinel-1 ascending dataset.**

*NOT CLASSIFIED*
*This document discloses subject matter in which e-GEOS has proprietary rights. Recipient of the document shall not duplicate, use or disclose in whole or in part, information contained herein except for or on behalf of e-GEOS to fulfil the purpose for which the document was delivered to him.*

| Sentinel-1 Descending | | | | | | | | | | | | | | | |
|---|---|---|---|---|---|---|---|---|---|---|---|---|---|---|---|
| 1 | 30/03/2015 | 51 | 13/11/2016 | 101 | 09/09/2017 | 151 | 06/07/2018 | 201 | 20/05/2019 | 251 | 21/03/2020 | 301 | 15/01/2021 | | |
| 2 | 23/04/2015 | 52 | 19/11/2016 | 102 | 15/09/2017 | 152 | 12/07/2018 | 202 | 26/05/2019 | 252 | 27/03/2020 | 302 | 21/01/2021 | | |
| 3 | 05/05/2015 | 53 | 25/11/2016 | 103 | 21/09/2017 | 153 | 18/07/2018 | 203 | 01/06/2019 | 253 | 02/04/2020 | 303 | 27/01/2021 | | |
| 4 | 17/05/2015 | 54 | 01/12/2016 | 104 | 27/09/2017 | 154 | 24/07/2018 | 204 | 13/06/2019 | 254 | 08/04/2020 | 304 | 02/02/2021 | | |
| 5 | 29/05/2015 | 55 | 07/12/2016 | 105 | 03/10/2017 | 155 | 30/07/2018 | 205 | 19/06/2019 | 255 | 14/04/2020 | 305 | 08/02/2021 | | |
| 6 | 10/06/2015 | 56 | 13/12/2016 | 106 | 09/10/2017 | 156 | 05/08/2018 | 206 | 25/06/2019 | 256 | 20/04/2020 | 306 | 14/02/2021 | | |
| 7 | 04/07/2015 | 57 | 19/12/2016 | 107 | 15/10/2017 | 157 | 11/08/2018 | 207 | 01/07/2019 | 257 | 26/04/2020 | 307 | 20/02/2021 | | |
| 8 | 16/07/2015 | 58 | 25/12/2016 | 108 | 21/10/2017 | 158 | 17/08/2018 | 208 | 07/07/2019 | 258 | 02/05/2020 | 308 | 26/02/2021 | | |
| 9 | 28/07/2015 | 59 | 31/12/2016 | 109 | 27/10/2017 | 159 | 23/08/2018 | 209 | 13/07/2019 | 259 | 08/05/2020 | 309 | 04/03/2021 | | |
| 10 | 09/08/2015 | 60 | 06/01/2017 | 110 | 02/11/2017 | 160 | 04/09/2018 | 210 | 19/07/2019 | 260 | 14/05/2020 | 310 | 10/03/2021 | | |
| 11 | 21/08/2015 | 61 | 12/01/2017 | 111 | 08/11/2017 | 161 | 10/09/2018 | 211 | 25/07/2019 | 261 | 20/05/2020 | 311 | 16/03/2021 | | |
| 12 | 02/09/2015 | 62 | 18/01/2017 | 112 | 14/11/2017 | 162 | 16/09/2018 | 212 | 31/07/2019 | 262 | 26/05/2020 | 312 | 22/03/2021 | | |
| 13 | 14/09/2015 | 63 | 24/01/2017 | 113 | 20/11/2017 | 163 | 22/09/2018 | 213 | 06/08/2019 | 263 | 01/06/2020 | 313 | 28/03/2021 | | |
| 14 | 26/09/2015 | 64 | 30/01/2017 | 114 | 26/11/2017 | 164 | 28/09/2018 | 214 | 12/08/2019 | 264 | 07/06/2020 | 314 | 03/04/2021 | | |
| 15 | 08/10/2015 | 65 | 05/02/2017 | 115 | 02/12/2017 | 165 | 04/10/2018 | 215 | 18/08/2019 | 265 | 13/06/2020 | 315 | 09/04/2021 | | |
| 16 | 01/11/2015 | 66 | 11/02/2017 | 116 | 08/12/2017 | 166 | 10/10/2018 | 216 | 24/08/2019 | 266 | 19/06/2020 | 316 | 15/04/2021 | | |
| 17 | 13/11/2015 | 67 | 17/02/2017 | 117 | 14/12/2017 | 167 | 16/10/2018 | 217 | 30/08/2019 | 267 | 25/06/2020 | 317 | 21/04/2021 | | |
| 18 | 25/11/2015 | 68 | 23/02/2017 | 118 | 20/12/2017 | 168 | 22/10/2018 | 218 | 05/09/2019 | 268 | 01/07/2020 | 318 | 27/04/2021 | | |
| 19 | 07/12/2015 | 69 | 01/03/2017 | 119 | 26/12/2017 | 169 | 28/10/2018 | 219 | 11/09/2019 | 269 | 07/07/2020 | 319 | 03/05/2021 | | |
| 20 | 19/12/2015 | 70 | 07/03/2017 | 120 | 01/01/2018 | 170 | 03/11/2018 | 220 | 17/09/2019 | 270 | 13/07/2020 | 320 | 09/05/2021 | | |
| 21 | 31/12/2015 | 71 | 13/03/2017 | 121 | 07/01/2018 | 171 | 09/11/2018 | 221 | 23/09/2019 | 271 | 19/07/2020 | 321 | 15/05/2021 | | |
| 22 | 12/01/2016 | 72 | 19/03/2017 | 122 | 13/01/2018 | 172 | 15/11/2018 | 222 | 29/09/2019 | 272 | 25/07/2020 | 322 | 21/05/2021 | | |
| 23 | 24/01/2016 | 73 | 25/03/2017 | 123 | 19/01/2018 | 173 | 21/11/2018 | 223 | 05/10/2019 | 273 | 31/07/2020 | 323 | 27/05/2021 | | |
| 24 | 05/02/2016 | 74 | 31/03/2017 | 124 | 25/01/2018 | 174 | 27/11/2018 | 224 | 11/10/2019 | 274 | 06/08/2020 | 324 | 02/06/2021 | | |
| 25 | 17/02/2016 | 75 | 06/04/2017 | 125 | 31/01/2018 | 175 | 03/12/2018 | 225 | 17/10/2019 | 275 | 12/08/2020 | 325 | 08/06/2021 | | |
| 26 | 29/02/2016 | 76 | 12/04/2017 | 126 | 06/02/2018 | 176 | 09/12/2018 | 226 | 23/10/2019 | 276 | 18/08/2020 | 326 | 14/06/2021 | | |
| 27 | 12/03/2016 | 77 | 18/04/2017 | 127 | 12/02/2018 | 177 | 15/12/2018 | 227 | 29/10/2019 | 277 | 24/08/2020 | 327 | 20/06/2021 | | |
| 28 | 24/03/2016 | 78 | 24/04/2017 | 128 | 18/02/2018 | 178 | 21/12/2018 | 228 | 04/11/2019 | 278 | 30/08/2020 | 328 | 26/06/2021 | | |
| 29 | 05/04/2016 | 79 | 30/04/2017 | 129 | 24/02/2018 | 179 | 27/12/2018 | 229 | 10/11/2019 | 279 | 05/09/2020 | 329 | 02/07/2021 | | |
| 30 | 17/04/2016 | 80 | 06/05/2017 | 130 | 02/03/2018 | 180 | 02/01/2019 | 230 | 16/11/2019 | 280 | 11/09/2020 | 330 | 08/07/2021 | | |
| 31 | 29/04/2016 | 81 | 12/05/2017 | 131 | 08/03/2018 | 181 | 08/01/2019 | 231 | 22/11/2019 | 281 | 17/09/2020 | 331 | 14/07/2021 | | |
| 32 | 11/05/2016 | 82 | 18/05/2017 | 132 | 14/03/2018 | 182 | 14/01/2019 | 232 | 28/11/2019 | 282 | 23/09/2020 | 332 | 20/07/2021 | | |
| 33 | 23/05/2016 | 83 | 24/05/2017 | 133 | 20/03/2018 | 183 | 20/01/2019 | 233 | 04/12/2019 | 283 | 29/09/2020 | 333 | 26/07/2021 | | |
| 34 | 04/06/2016 | 84 | 30/05/2017 | 134 | 26/03/2018 | 184 | 26/01/2019 | 234 | 10/12/2019 | 284 | 05/10/2020 | 334 | 01/08/2021 | | |
| 35 | 16/06/2016 | 85 | 05/06/2017 | 135 | 01/04/2018 | 185 | 13/02/2019 | 235 | 16/12/2019 | 285 | 11/10/2020 | | | | |
| 36 | 28/06/2016 | 86 | 11/06/2017 | 136 | 07/04/2018 | 186 | 19/02/2019 | 236 | 22/12/2019 | 286 | 17/10/2020 | | | | |
| 37 | 10/07/2016 | 87 | 17/06/2017 | 137 | 13/04/2018 | 187 | 25/02/2019 | 237 | 28/12/2019 | 287 | 23/10/2020 | | | | |
| 38 | 22/07/2016 | 88 | 23/06/2017 | 138 | 19/04/2018 | 188 | 03/03/2019 | 238 | 03/01/2020 | 288 | 29/10/2020 | | | | |
| 39 | 15/08/2016 | 89 | 29/06/2017 | 139 | 25/04/2018 | 189 | 09/03/2019 | 239 | 09/01/2020 | 289 | 04/11/2020 | | | | |
| 40 | 27/08/2016 | 90 | 05/07/2017 | 140 | 01/05/2018 | 190 | 15/03/2019 | 240 | 15/01/2020 | 290 | 10/11/2020 | | | | |
| 41 | 08/09/2016 | 91 | 11/07/2017 | 141 | 07/05/2018 | 191 | 21/03/2019 | 241 | 21/01/2020 | 291 | 16/11/2020 | | | | |
| 42 | 20/09/2016 | 92 | 17/07/2017 | 142 | 13/05/2018 | 192 | 27/03/2019 | 242 | 27/01/2020 | 292 | 22/11/2020 | | | | |
| 43 | 26/09/2016 | 93 | 23/07/2017 | 143 | 19/05/2018 | 193 | 02/04/2019 | 243 | 02/02/2020 | 293 | 28/11/2020 | | | | |
| 44 | 02/10/2016 | 94 | 29/07/2017 | 144 | 25/05/2018 | 194 | 08/04/2019 | 244 | 08/02/2020 | 294 | 04/12/2020 | | | | |
| 45 | 08/10/2016 | 95 | 04/08/2017 | 145 | 31/05/2018 | 195 | 14/04/2019 | 245 | 14/02/2020 | 295 | 10/12/2020 | | | | |
| 46 | 14/10/2016 | 96 | 10/08/2017 | 146 | 06/06/2018 | 196 | 20/04/2019 | 246 | 20/02/2020 | 296 | 16/12/2020 | | | | |
| 47 | 20/10/2016 | 97 | 16/08/2017 | 147 | 12/06/2018 | 197 | 26/04/2019 | 247 | 26/02/2020 | 297 | 22/12/2020 | | | | |
| 48 | 26/10/2016 | 98 | 22/08/2017 | 148 | 18/06/2018 | 198 | 02/05/2019 | 248 | 03/03/2020 | 298 | 28/12/2020 | | | | |
| 49 | 01/11/2016 | 99 | 28/08/2017 | 149 | 24/06/2018 | 199 | 08/05/2019 | 249 | 09/03/2020 | 299 | 03/01/2021 | | | | |
| 50 | 07/11/2016 | ## | 03/09/2017 | 150 | 30/06/2018 | 200 | 14/05/2019 | 250 | 15/03/2020 | 300 | 09/01/2021 | | | | |

**Table 3: acquisition dates (dd/mm/yyyy) of the analyzed SAR images – Sentinel-1 descending dataset.**

*NOT CLASSIFIED*
*This document discloses subject matter in which e-GEOS has proprietary rights. Recipient of the document shall not duplicate, use or disclose in whole or in part, information contained herein except for or on behalf of e-GEOS to fulfil the purpose for which the document was delivered to him.*

| TerraSAR-X Descending | | | | | |
|---|---|---|---|---|---|
| 1 | 13/06/2014 | 21 | 04/03/2015 | 41 | 21/10/2015 |
| 2 | 24/06/2014 | 22 | 26/03/2015 | 42 | 12/11/2015 |
| 3 | 05/07/2014 | 23 | 06/04/2015 | 43 | 23/11/2015 |
| 4 | 16/07/2014 | 24 | 17/04/2015 | 44 | 04/12/2015 |
| 5 | 27/07/2014 | 25 | 28/04/2015 | 45 | 15/12/2015 |
| 6 | 18/08/2014 | 26 | 09/05/2015 | 46 | 26/12/2015 |
| 7 | 29/08/2014 | 27 | 20/05/2015 | 47 | 06/01/2016 |
| 8 | 09/09/2014 | 28 | 31/05/2015 | 48 | 17/01/2016 |
| 9 | 20/09/2014 | 29 | 11/06/2015 | 49 | 08/02/2016 |
| 10 | 01/10/2014 | 30 | 22/06/2015 | 50 | 19/02/2016 |
| 11 | 12/10/2014 | 31 | 03/07/2015 | 51 | 01/03/2016 |
| 12 | 23/10/2014 | 32 | 14/07/2015 | 52 | 12/03/2016 |
| 13 | 03/11/2014 | 33 | 25/07/2015 | 53 | 23/03/2016 |
| 14 | 14/11/2014 | 34 | 05/08/2015 | | |
| 15 | 25/11/2014 | 35 | 16/08/2015 | | |
| 16 | 06/12/2014 | 36 | 27/08/2015 | | |
| 17 | 28/12/2014 | 37 | 07/09/2015 | | |
| 18 | 08/01/2015 | 38 | 18/09/2015 | | |
| 19 | 30/01/2015 | 39 | 29/09/2015 | | |
| 20 | 10/02/2015 | 40 | 10/10/2015 | | |

**Table 4: acquisition dates (dd/mm/yyyy) of the analyzed SAR images – TerraSAR-X descending dataset.**

*NOT CLASSIFIED*
*This document discloses subject matter in which e-GEOS has proprietary rights. Recipient of the document shall not duplicate, use or disclose in whole or in part, information contained herein except for or on behalf of e-GEOS to fulfil the purpose for which the document was delivered to him.*

### *Sentinel-1 constellation – European Space Agency*

Sentinel-1 mission is part of the Copernicus program, with a partnership between ESA (European Space Agency) and European Commission, representing a revolution in the Earth Observation scientific world.
Sentinel-1 is a two-satellite constellation with the prime objectives of Land and Ocean monitoring. The goal of the mission is to provide C-Band SAR data continuity following the retirement of ERS-2 and the end of the Envisat mission. The first satellite (Sentinel-1A) launch occurred on 03 April 2014, meanwhile the second one (Sentinel-1B) was launched two years later.
Both satellites carry onboard a C-band SAR sensor (5,40 GHz frequency and about 5,55 cm wavelength), able to acquire SAR images with extremely variable resolution and coverage (up to 400 km of swath). Specifically, the standard acquisition mode is the Interferometric Wide Swath (IW), characterized by 250 km wide images and resolution comparable to the first-generation ESA satellites (ERS and Envisat). Such effective performances are possible thanks to an innovative acquisition mode, called TOPS (Terrain Observation with Progressive Scans SAR). One of the main advantages of Sentinel-1 is the short revisit time, that is 12 days (or 6 days with the acquisition of both satellites over the same area).

### *TerraSAR-X/TanDEM-X constellation – Deutsches Zentrum für Luft- und Raumfahrt*

TerraSAR-X/TanDEM-X is a high-resolution interferometric X-band SAR mission of DLR (German Aerospace Center), together with the partners EADS Astrium GmbH and Infoterra GmbH. The mission concept is based on a second TerraSAR-X (TSX) radar satellite flying in close formation to achieve the desired interferometric baselines in a highly reconfigurable constellation. The first satellite launch occurred on 15 June 2007, while the second one was launched three years later, on 21 June 2010. Beyond its primary mission objective of generating a global HRTI-3 DEM, TanDEM-X provides a configurable SAR interferometry platform for SAR techniques and applications, such as digital beamforming, single-pass polarimetric SAR interferometry, ATI (Along-Track Interferometry) with varying baseline.
Both satellites carry onboard an X-band SAR sensor (9,65 GHz frequency and 3,1 cm wavelength), able to acquire SAR images with variable incidence angle (15° to 60°), polarization (single, dual, quad) resolution (from 1m x 1m to 16m x 16m), footprint (from 5km x 10 km to ≤ 1500 km x 30 km) according to different SAR modes (Stripmap, ScanSAR, Spotlight). One of the main advantages of TerraSAR-X is the possibility to achieve high-resolution interferometric (e.g., 3m x 3m in Stripmap mode).

*NOT CLASSIFIED*
*This document discloses subject matter in which e-GEOS has proprietary rights. Recipient of the document shall not duplicate, use or disclose in whole or in part, information contained herein except for or on behalf of e-GEOS to fulfil the purpose for which the document was delivered to him.*

# 5. Type of analysis performed, including the operating principles of the algorithms

The basic philosophy that led to the execution of the activities is based on the awareness that phenomena able to generate structural displacements and deformations of bridges have specific peculiarities, both in terms of spatial and temporal evolution, depending on several variables and factors, especially considering the different types of bridges in the study area. Considering the needs of the client to understand whether InSAR can determine the deformations of bridges in a reliable way and with sufficient detail and accuracy (especially regarding the location of measurement points), a customized approach was implemented.

The project concerns the analysis of high-resolution SAR data collected from TerraSAR-X satellite, and medium resolution SAR data collected from Sentinel-1 constellation. These analyses were carried out according to two levels of detail:

1) a first level of "InSAR screening analyses" ("wide area level") extended to the whole area of analysis requested by the Client;

2) a second level of processing, the so called "InSAR focus analyses", related to detailed site-specific analyses carried out for the bridges of interest.

During the PoC, the InSAR focus analyses were implemented for the 20 bridges of interest. The InSAR focus approach has been customized in order to be scaled up and applied over the wider area requested in the implementation phase to obtain a detailed analysis of all the 600 bridges.

The "InSAR Screening Analyses" were performed over the whole area of interest. For the Sentinel-1 datasets, the analyses included the use of proprietary software (PSP-IFSAR developed by e-GEOS), tools and proprietary post-processing algorithms. For the TerraSAR-X dataset, the analyses followed the A-DInSAR principles adopted by NHAZCA for the processing and post-processing activities.

The multi-temporal A-DInSAR analyses have been performed by means of a workflow that is adaptable to this specific case and the characteristics of the area of interest, the evolution of observed processes, the typology of the SAR images and other auxiliary data. The InSAR screening step allowed to generate velocity maps and time series of deformations of radar targets (measurement points) by using differential interferograms obtained from InSAR pairs.

The processing chains adopted for the Sentinel-1 datasets (*PSP-IFSAR*) were fully automated, and they interfaced with a database storing the input data, the intermediate and the final products. The SAR data processing chains were equipped with an internal process control to guarantee high quality results.

In summary, the workflow of the A-DInSAR analyses adopted for the Sentinel-1 and TerraSAR-

***NOT CLASSIFIED***
***This document discloses subject matter in which e-GEOS has proprietary rights. Recipient of the document shall not duplicate, use or disclose in whole or in part, information contained herein except for or on behalf of e-GEOS to fulfil the purpose for which the document was delivered to him.***

X datasets included the following steps:

- Data retrieval:
  - SAR images in SLC (Single Look Complex) format, characterized by the highest spatial resolution and including the phase parameter, which is fundamental to carry out interferometric analyses;
  - digital elevation model (EU-DEM) to be used in radar coordinates;
  - precise orbital data;
- InSAR pre-processing:
  - identification of the master image to minimize the decorrelation effects;
  - co-registration of all the slave images;
  - analysis of the amplitude time series and check of every single image to discard potential corrupted data that could affect interferometric processing;
  - interferogram formation with eventual multi-temporal adaptive filters, able to maximize the coherence value without influencing the spatial resolution and optimizing the response of individual radar targets on the scene;
- A-DInSAR processing:
  - tuning of the processing parameters (reflectivity, amplitude stability index, interferometric coherence, graph connectivity) to obtain a reliable result in terms of signal to noise ratio;
  - preliminary identification of measurement points;
  - reconstruction of models for the spatial and temporal connections (e.g. linear and nonlinear and/or cyclic deformation) to optimize the results achievable according to the topographical, environmental and kinematics characteristics of the processes under investigation;
  - phase unwrapping: the components of the deformation not described by the deformation model can be retrieved by unwrapping the interferometric phase residuals. The phase of the SAR signal is measured modulo $2\pi$, that is it assumes values in the range $[-\pi,]$. The objective of the phase unwrapping is to solve this ambiguity, estimating the absolute (unwrapped) phase of every PS, adding the correct number of cycles to the wrapped phase.
  - removal of the orbital and atmospheric disturbances: estimation spatially low varying and temporally decorrelated functions describing residual errors due to orbital accuracy, atmospheric stratification and turbulent component;
  - selection of the reference point, also with respect to the geomorphological and cinematic context;
  - projection of results on GIS system on orthophotos and topographic maps;
- Quality controls:
  - analysis of the time series of displacement with respect to the acquisition geometry and the deformation process;
  - reliability check of the geographic coordinates and estimated residual heights with respect to the DEM.

*NOT CLASSIFIED*
*This document discloses subject matter in which e-GEOS has proprietary rights. Recipient of the document shall not duplicate, use or disclose in whole or in part, information contained herein except for or on behalf of e-GEOS to fulfil the purpose for which the document was delivered to him.*

The "InSAR Focus Analyses" allowed to perform detailed and site-specific analyses and control of measurement points. These analyses were performed for the bridges of interest and for specific limited areas affected by relevant and/or localized deformation processes detected during the InSAR Screening step.
The analyses were performed using proprietary software and tools organized in modular structures allowing a large flexibility to operate on the "raw" data, thus applying different methodologies according to the characteristics of the specific process under investigation among which: i) analysis module of amplitude and reflectivity data; ii) analysis of temporary scatterers (to further increase the sample of potential measurement points by exploiting newborn targets and/or coherent targets for specific time intervals); iii) analysis with different deformation models (e.g., non-linear); iv) localized area analyses, allowing to reduce the atmospheric noise for small-scale analysis.

The InSAR processing has been performed with specific auxiliary data for the basic geographic information and geocoding of results: the EU-DEM, a Digital Elevation Model (DEM) with a 25 m resolution cell and a vertical accuracy of +/- 7 m RMSE, has been adopted. The EU-DEM derives from DEM fusion techniques combining data from different sources into a single, consistent and homogeneous elevation dataset. The fusion process relied on data from ASTER GDEM, SRTM and freely available Russian topomap series. The product is further edited to ensure that water features are adequately represented (information from http://land.copernicus.eu).

As for many geodetic techniques (e.g., levelling, GNSS), PS measurements are relative to a reference point in space (RP) - usually referred to as P0 - and a reference date in time (RT). The temporal reference (RT) can be chosen at will among the acquisition dates without changing the shape of the time series, besides a mere shift: however, the noise component affecting the SAR image acquired at the date used as reference can create a constant shift of the time series. To mitigate the possible impact of unfavorable choices of the RT and to limit the impact of noise components overlying the data, the approach taken for the Sentinel-1 analyses is to refer each time series to the origin of the regression model used to estimate the temporal coherence of the PS, which is a third-order polynomial plus a seasonal component with a period of 1 year. Therefore, after applying the regression, each time series is shifted by the constant, and can begin from a value different from zero at the first date. Conversely, for the TerraSAR-X products the SAR images have been referred to a master image (selected to optimize the temporal and the normal baselines) for the phase difference computations and the temporal reference point is referred to the first acquisition date (T0).
As the phase difference computations are differential (i.e., they do not express an absolute value of displacement over time, but a relative displacement with respect to a reference point), spatial reference can be obtained through the choice of a particular PS (RP), which is considered as motionless and whose measured displacement is then subtracted to each single PS. This approach results in a dataset where RP has a displacement identically null, while all the other PSs are assigned displacements that are the deviation of their displacement from RP: this means that all the noise affecting RP is then reproduced in every PS displacement.

*NOT CLASSIFIED*
*This document discloses subject matter in which e-GEOS has proprietary rights. Recipient of the document shall not duplicate, use or disclose in whole or in part, information contained herein except for or on behalf of e-GEOS to fulfil the purpose for which the document was delivered to him.*

For the Sentinel-1 datasets and analyses, the chosen approach is to estimate a "virtual" RP displacement: at each date, the displacement of the "virtual" RP is computed so that the global displacement at said date can be considered null. It's important to be aware that this approach is feasible only if the area under investigation is not affected by a global movement. By subtracting the displacement of this "virtual" RP from all the PSs, the impact of measurement noise on a single measurement is strongly mitigated. Regarding the TerraSAR-X dataset and analysis, the reference point was represented by a point within the investigated area that is assumed as stable (not affected by movement). Therefore, in order to perform differential displacement analyses, the reference point has been selected in in an area in correspondence to the GNSS station "BRUX00BEL" (EUREF network, Royal Observatory of Belgium, https://epncb.eu), which showed absence of relevant displacements in the vertical direction in the investigated period. The identification of the reference point on satellite optical image and its geographic coordinates are reported in Figure 5.

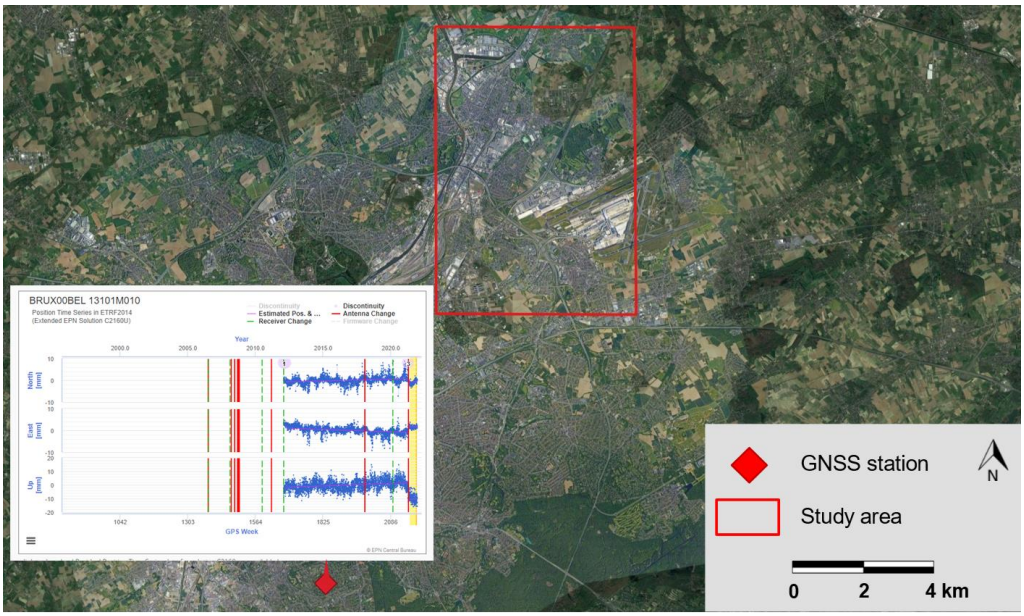


**Figure 5: identification of the reference point on satellite optical image (approximate coordinates: lat. 50.798°, lon. 4.359°). The station North, East and elevation historical time series is reported. An absence of long-term deformation is detected, with the exception of the last period, due to the change of the antenna.**

Starting from the results achieved by the above-described analyses, a post-processing and validation process has been performed. Specifically, semi-automatic validation routines based on statistical algorithms and software tools have been applied, allowing for a point-to-point multi-parameter control of all the available measurement points aiming at analyzing the spatial and temporal deformational behaviours and to identify and remove unreliable outliers.

*NOT CLASSIFIED*
*This document discloses subject matter in which e-GEOS has proprietary rights. Recipient of the document shall not duplicate, use or disclose in whole or in part, information contained herein except for or on behalf of e-GEOS to fulfil the purpose for which the document was delivered to him.*

# 6. Delivering of the achieved results TerraSAR-X and Sentinel-1

In the present report, the deformation rates of the Measurement Points (MP) is reported over orthophotographic basemaps, showing the average velocity of displacement (in mm/year) over the entire period of analysis. A color scale has been adopted to represent the velocity measured along the instrumental line of sight (LOS):

i) MPs moving away from the sensor are represented in yellow and red colors;
ii) MPs approaching the sensor are represented in cyan and blue colors;
iii) MPs with negligible displacements are represented in green color.

The MP displacement accuracy is about ±1.0 mm/yr for both Sentinel-1 Ascending/Descending and TerraSAR-X datasets.

The position accuracy is:

- TerraSAR-X: 0.5 m East; 1 m North; 0.5 m Elevation;
- Sentine-1: 9 m East; 6 m North; 7 m Elevation;

In addition, the Sentinel-1 and TerraSAR-X products are delivered also in the ESRI shapefile format, a digital geodatabase format compatible with GIS software, and into the AWARE platform.

The geodatabase contains the following information for each measurement point (MP):

- **MP code**: unique identification alphanumeric code;
- **PS position:** the PS position, in geographic coordinates expressed in WGS84 (EPSG:4326) and Belgian Lambert 72 (EPSG:31370). The measurements of the PS positions are relative. In order to better understand the correspondence of the PS with the object on the ground, the absolute position is obtained aligning the detected PS position with the available cartography, orthophotos, etc. In the absence of this information, the Google Earth orthoimages are used as absolute reference;
- **MP effective area**: the size of the area represented by the MP, expressed in number of averaged resolution cells. If the MP is a PS, this field has value 1; if the MP is a DS, this field is higher than 1. In this way, it is possible to consult both collectively and individually PS/DS by applying a simple selection filter;
- **MP Structure ID**: an alphanumeric code with the first characters indicates if a point belongs (“B”) to a bridge, not belonging to a bridge (“0”) or it is uncertain (“U”) and others two characters representing the infrastructure;
- **MP temporal coherence**: quality index associated to the MP, defined in the range [0, 1]; it measures the goodness of the model with respect to the actual displacement;

*NOT CLASSIFIED*
*This document discloses subject matter in which e-GEOS has proprietary rights. Recipient of the document shall not duplicate, use or disclose in whole or in part, information contained herein except for or on behalf of e-GEOS to fulfil the purpose for which the document was delivered to him.*

- **MP average velocity**: average velocity, expressed in mm/year, during the period between the first and the last SAR acquisition dates. The displacement is measured along the line of sight of the sensor and are referred back to a reference PS (or an area), assumed motionless;
- **MP average velocity standard deviation**. This field represents the standard deviation of the estimated average velocity, expressed in mm/year.
- **MP average acceleration**: average displacement acceleration, expressed in mm/year2, during the period between the first and the last SAR acquisition dates. The acceleration is measured along the line of sight of the sensor and it is referred back to a reference PS (or an area), assumed motionless;
- **MP average acceleration standard deviation**. This field represents the standard deviation of the estimated average acceleration, expressed in mm/year2.
- **MP height**: elevation of the MP expressed in mTAW.
- **MP height standard deviation**. This field represents the standard deviation of the estimated height, expressed in m.
- **MP displacement time series**: the measured displacement, expressed in mm, measured on each acquisition date over the analyzed period. The displacement is measured along the line of sight of the sensor and are referred back to a reference PS (or an area), assumed motionless, and to a reference date (among the acquisition dates, typically the first one).
- **MP displacement RMSE**: the estimated root mean square error, expressed in mm, associated to the displacement. The estimation is carried out considering the residual with respect to a model of the displacement used in the PSI processing
- **MP average velocity (no thermal dilatation):** average velocity, apart for annual oscillation component due to thermal dilatation, expressed in mm/year, during the period between the first and the last SAR acquisition dates. The displacement is measured along the line of sight of the sensor and are referred back to a reference PS (or an area), assumed motionless;
- **MP average annual oscillation amplitude**: the amplitude of the oscillation, with a period of one year, correlated with the temperature variation along the whole analyzed period. The oscillation amplitude is measured in mm along the line of sight of the sensor and referred back to a reference PS (or an area), assumed motionless.

The delivery of results is provided also through an advanced WebGIS portal, called AWARE, developed by e-GEOS in order to support user analysis by providing tools enabling the user to generate additional information layers, specific to their analysis.
AWARE (Agile Monitoring of Assets and Resources) is a vertical application platform for the provision of products, services and advanced analytics tools supporting critical asset and infrastructure monitoring and management. AWARE is a secure cloud-based platform, founded on OpenSource developments and is compliant with all common OGC standards. External services that follow OGC standards should easily integrate with the platform. The platform is accessible 24 hours per day, 365 days per year through common internet browsers (e.g. Chrome, Firefox or Edge) and by mobile phone using the AWARE app downloadable

*NOT CLASSIFIED*
*This document discloses subject matter in which e-GEOS has proprietary rights. Recipient of the document shall not duplicate, use or disclose in whole or in part, information contained herein except for or on behalf of e-GEOS to fulfil the purpose for which the document was delivered to him.*

from the Google or Apple store. AWARE provides tools and instruments allowing the user to perform specific analysis on EO value added products, and generate reports. Integration of non-EO data (RPAS video and geotagged photo, third party's systems, meteorological information, on site sensors data, etc.) is also available. User-defined alerts to monitor specific phenomena can also be implemented.

A feature of the advanced AWARE portal is its support for ground deformation analysis, providing specific tools and functionalities to analyse data derived by satellite interferometric analysis, and enabling the user to analyse areas of interest at different scales, from single structure to whole areas. The manual for providing training to the use of the AWARE platform has been provided separately.

In the following table, a scheme of the attribute table of Sentinel-1 and TerraSAR-X is reported:

| | | Geodatabases attribute header |
|---|---|---|
| Code | | CODE |
| Latitude in WGS84 | | LAT_WGS84 |
| Longitude in WGS84 | | LON_WGS84 |
| Latitude in LAMBERT72 | | LAT_LAMB72 |
| Longitude in LAMBERT72 | | LON_LAMB72 |
| Effective area | | EFF_AREA |
| Structure ID | Bxx,U,0 | STRUCT_ID |
| Temporal Coherence | [0,1] | COHE |
| Average velocity | mm/year | VEL |
| Av. Vel. Standard Deviation | mm/year | V_STDEV |
| Average acceleration | mm/year^2 | ACC |
| Av. Acc. Standard Deviation | mm/year^2 | A_STDEV |
| Height in mTAW | mTAW | HEIGHT |
| Height in m.a.s.l. | m.a.s.l. | HGT_MASL |
| Height Standard Deviation | m | H_STDEV |
| Cumulative Displacement | mm | CUMUL.DISP |
| Displacement time series | mm | Dyyyymmdd |
| Displacement RMSE | mm | STDEV |
| Av. Vel. without Thermal Expansion | mm/year | VEL_NO_TE |
| Average Annual Oscillation Amplitude | mm | SEASONAL |
| Temporary Scatterers - date ON | nr. img | ON |
| Temporary Scatterers - date OFF | nr. img | OFF |

**Table 5: scheme of the attribute table of Sentinel-1 and TerraSAR-X delivered to the Client in ESRI shapefile format and shared through AWARE platform.**

*NOT CLASSIFIED*
*This document discloses subject matter in which e-GEOS has proprietary rights. Recipient of the document shall not duplicate, use or disclose in whole or in part, information contained herein except for or on behalf of e-GEOS to fulfil the purpose for which the document was delivered to him.*

# 7. Results

In this section the results achieved by the processing of the ascending Sentinel-1 Interferometric Wide SAR data acquired from February 2015 to August 2021 (ascending and descending orbital geometry) and TerraSAR-X Stripmap SAR data acquired from June 2014 to March 2016 (descending orbital geometry), are reported.
The following figures show a global view of the mean velocities relevant to the three datasets (Figure 6, Figure 7, Figure 8). The value of the velocity is represented with different colors ranging from to blue to the red according to the legend reported on the right of the image.
A-DInSAR technique has been applied in order to obtain information about past long-term deformation processes with millimeter accuracy, allowing to provide for each measurement point its trend of deformation along the LOS (in millimeters/year) and time series of displacement (in millimeters).
Regarding the analyses performed using Sentinel-1 data:

- For the ascending dataset, a total area of about 55 $km^2$ was analyzed and about 200,000 measurement points were obtained, with an average density of about 3,600 MP/$km^2$.
- For the descending dataset, a total area of about 55 $km^2$ was analyzed and about 170,000 measurement points were obtained, with an average density of about 3,100 MP/$km^2$.

Regarding the analyses performed using TerraSAR-X data:

- For the descending dataset, a total area of about 55 $km^2$ was analyzed and about 1,310,000 measurement points were obtained, with an average density of about 24,000 MP/$km^2$.

*Distributed Scatterers* (DS) have been processed for both TerraSAR-X and Sentinel-1 data. DSs add value over rural and scarcely vegetated areas, and since we are in a densely urbanized area, a total amount of about 20.000 DS were obtained for TerraSAR-X and Sentinel-1 data. DS are not present in correspondence of the bridges of interest or the close surrounding areas.

By the analysis of the MPs velocity maps achieved by TerraSAR-X (in descending orbital geometry), it can be highlighted that the area presents a portion subjected to uplift (ranging from +1 to +3 mm/yr). By literature resources and by the comparison with local morphology, this is can be mainly linked to the groundwater recharge process currently active in the framework of the AOI. However, the rest of the study area presents little to no long-term deformations, by analyses with both Sentinel-1 and TerraSAR-X.
The complete coverage (100%) of the bridges has been achieved with high-resolution TerraSAR-X data. A good coverage (95%) of the bridges has been carried out with medium-

*NOT CLASSIFIED*
*This document discloses subject matter in which e-GEOS has proprietary rights. Recipient of the document shall not duplicate, use or disclose in whole or in part, information contained herein except for or on behalf of e-GEOS to fulfil the purpose for which the document was delivered to him.*

resolution Sentinel-1 data: just one bridge (003186) is not covered by Sentinel-1, since the amplitude of the back scattering is very low in both geometries.
TerraSAR-X data allowed to estimate the height of each MP with high accuracy and allowing also to distinguish not only the MP belonging to te bridges, but also the different portions of each bridge, as we can see in Figure 11 and Figure 12, and deeply explained in Sect. 8.

The *Trend Change Detection* analysis, performed by proprietary algorithms developed by NHAZCA S.r.l. has been carried out and allows the identification of the main periods when most of MP, for each bridge, recorded accelerations.
The Trend Change Detection analysis conducted doesn't highlight relevant acceleration/deceleration of the deformational trend of the MPs, suggesting a linear and constant deformational behavior for the most of MPs, with the exception of seasonal thermal oscillation detected on some clusters of MPs.

It is worth noting that the displacement of the measurement points is detected along the **instrumental line of sight (LOS)**. This implies that the measured displacement is the projection of the real displacement vector along the sensor-target line. For vertical movements (e.g. subsidence), the actual displacement can be easily retrieved by basic trigonometric functions; if the target is affected also by horizontal displacements, the achieved measurement is the result of the projection of all the components on the LOS. By the use of SAR images collected by different orbital geometries (ascending and descending) it is possible to perform more complex post-processing analysis in order to estimate the horizontal and the vertical components of the actual displacement vector
By exploiting the availability of different orbital geometries, the integration of the ascending and descending ground deformation measurements is presented. The integration procedure aims to retrieve the vertical and horizontal (East-West) component of the mean velocity and the deformations at the different acquisition dates starting from the mean velocities measured with the two acquisition geometries (ascending and descending). In Figure 8 and Figure 9, the vertical and the East-West components of the mean velocity over homologous points are reported. Positive values of the vertical mean velocity component indicate that the terrain lifts; positive values of the mean velocity along East-West direction indicate that the terrain moves towards East.
Specifically, the area was discretized in cells on a regular grid (a 50m × 50m cell) and results are achieved for the only cells containing at least one MP from the ascending stack and one MP from the descending one.
In addition, for vertical and horizontal displacement decomposition products, a unique result derived from both satellite measurements has been computed. Sentinel-1 and TerraSAR-X results have been inter-calibrated and merged in cells on a regular grid (a 30m × 30m cell) and reported in AWARE platform.

*NOT CLASSIFIED*
*This document discloses subject matter in which e-GEOS has proprietary rights. Recipient of the document shall not duplicate, use or disclose in whole or in part, information contained herein except for or on behalf of e-GEOS to fulfil the purpose for which the document was delivered to him.*

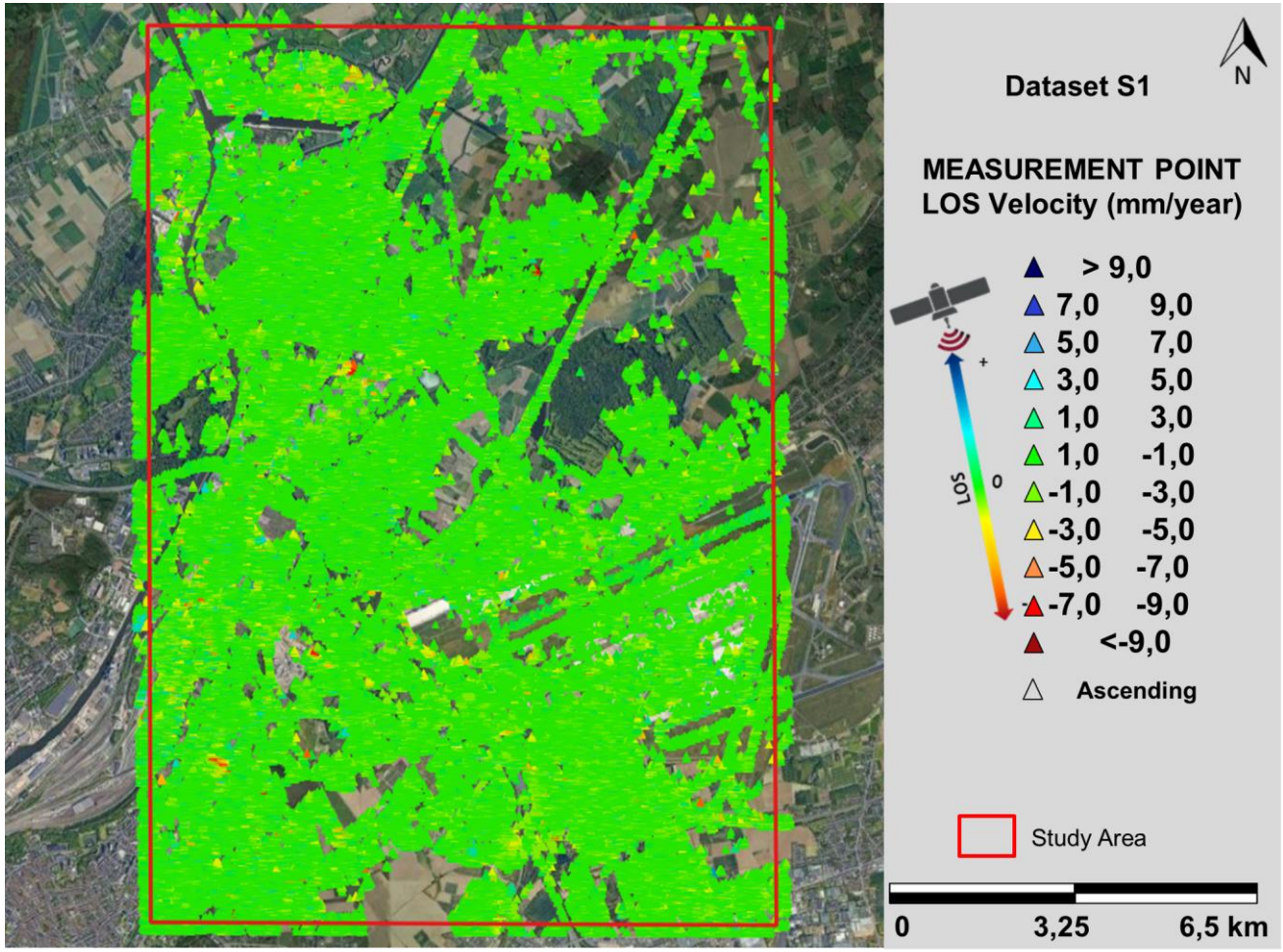


**Figure 6: The MP mean velocity map in ascending geometry relevant to the period February 2015 - July 2021, obtained by the PSP-IFSAR technique. The ascending stack is constituted by 325 Sentinel-1 Interferometric Wide SAR images, over in Brussels, Belgium. The PS measurements are superimposed to an optical image.**

*NOT CLASSIFIED*
*This document discloses subject matter in which e-GEOS has proprietary rights. Recipient of the document shall not duplicate, use or disclose in whole or in part, information contained herein except for or on behalf of e-GEOS to fulfil the purpose for which the document was delivered to him.*

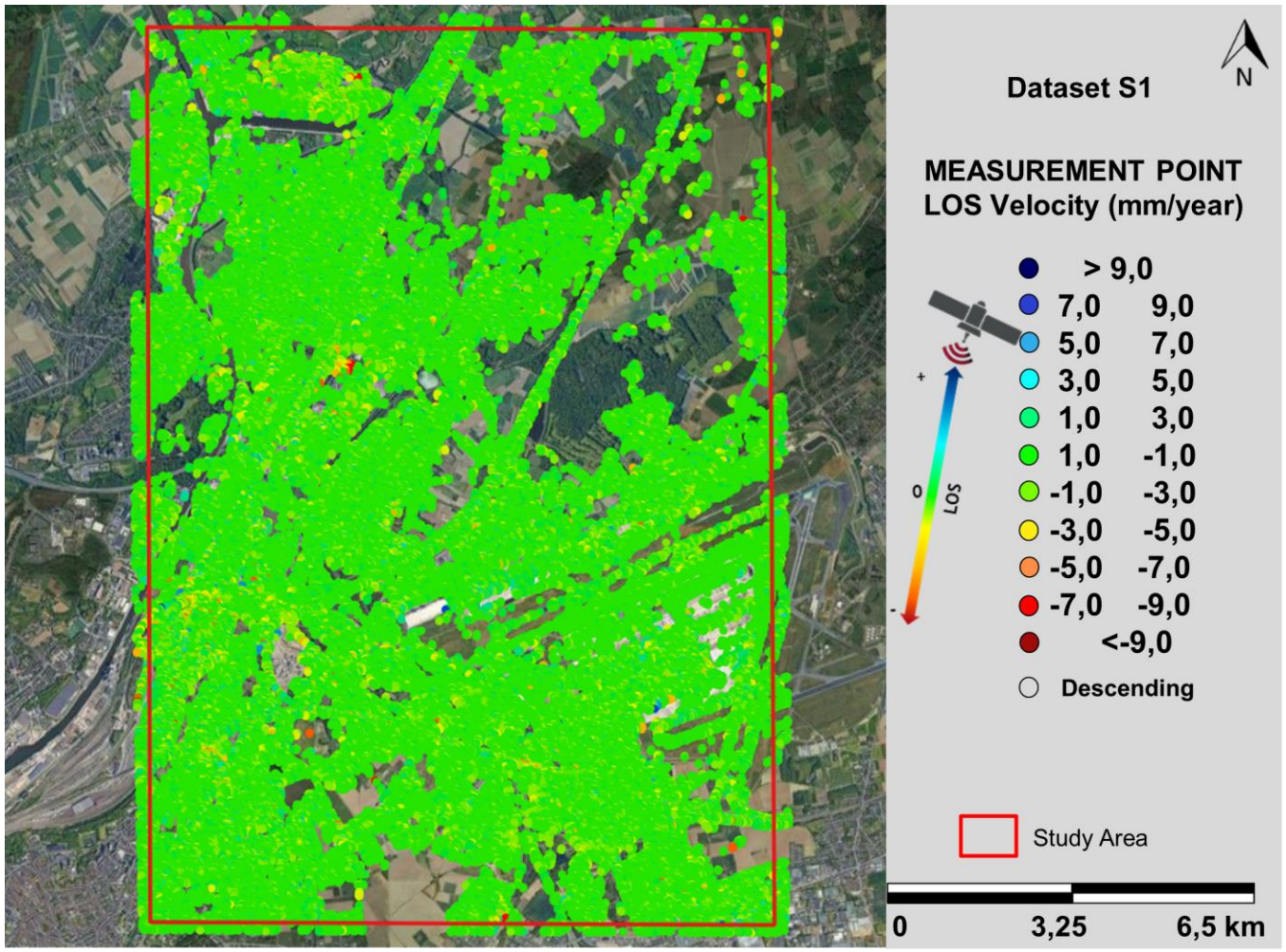


**Figure 7 The MP mean velocity map in descending geometry relevant to the period March 2015 - August 2021, obtained by the PSP-IFSAR technique. The descending stack is constituted by 334 Sentinel-1 Interferometric Wide SAR images, over Brussels, Belgium. The PS measurements are superimposed to an optical image.**

*NOT CLASSIFIED*
*This document discloses subject matter in which e-GEOS has proprietary rights. Recipient of the document shall not duplicate, use or disclose in whole or in part, information contained herein except for or on behalf of e-GEOS to fulfil the purpose for which the document was delivered to him.*

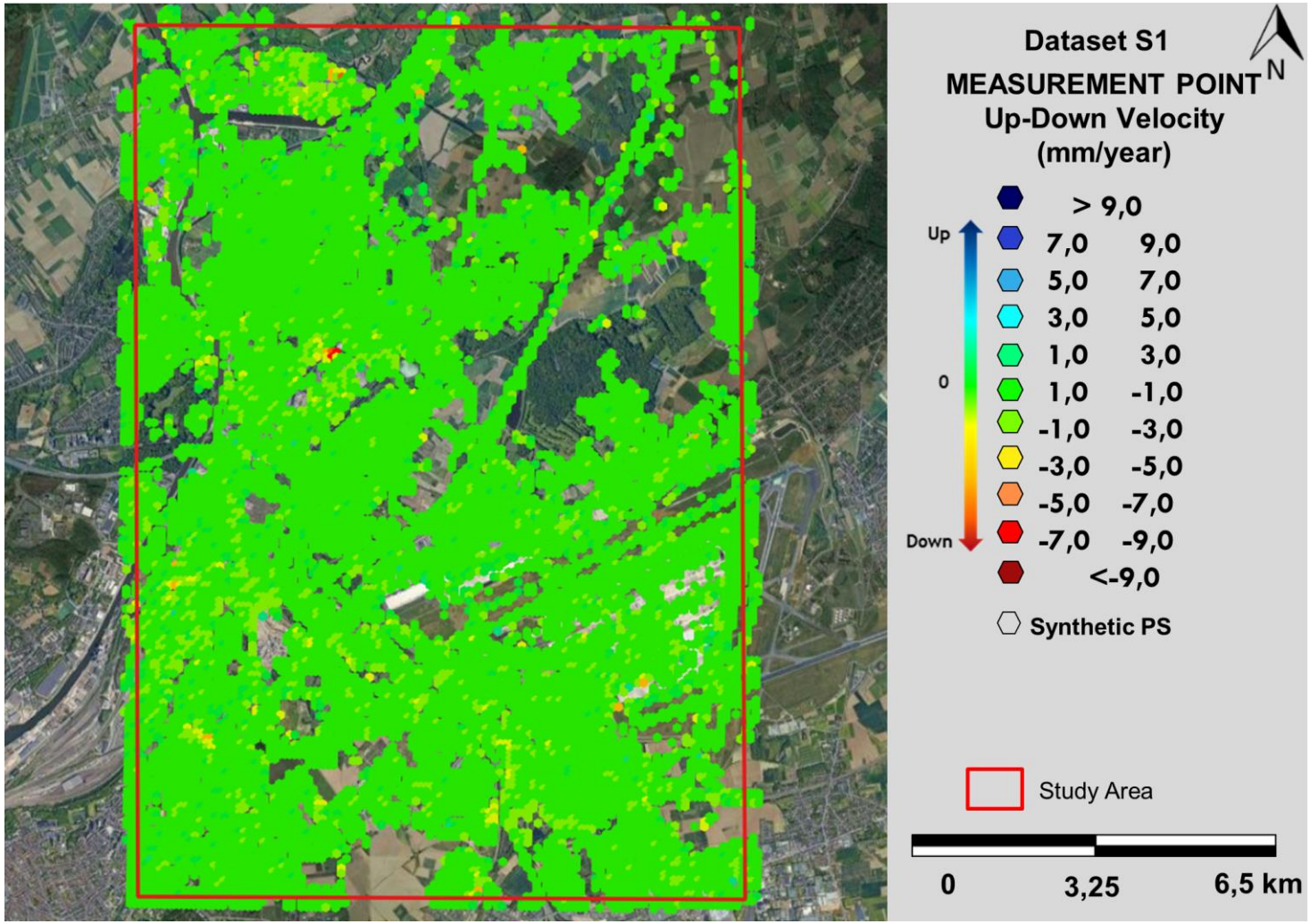


**Figure 8: The vertical component of the mean velocity obtained with the Sentinel-1 ascending and descending ground deformation measurements integration, relevant to the period March 2015 - July 2021. The obtained measurements are superimposed to an optical image.**

*NOT CLASSIFIED*
*This document discloses subject matter in which e-GEOS has proprietary rights. Recipient of the document shall not duplicate, use or disclose in whole or in part, information contained herein except for or on behalf of e-GEOS to fulfil the purpose for which the document was delivered to him.*

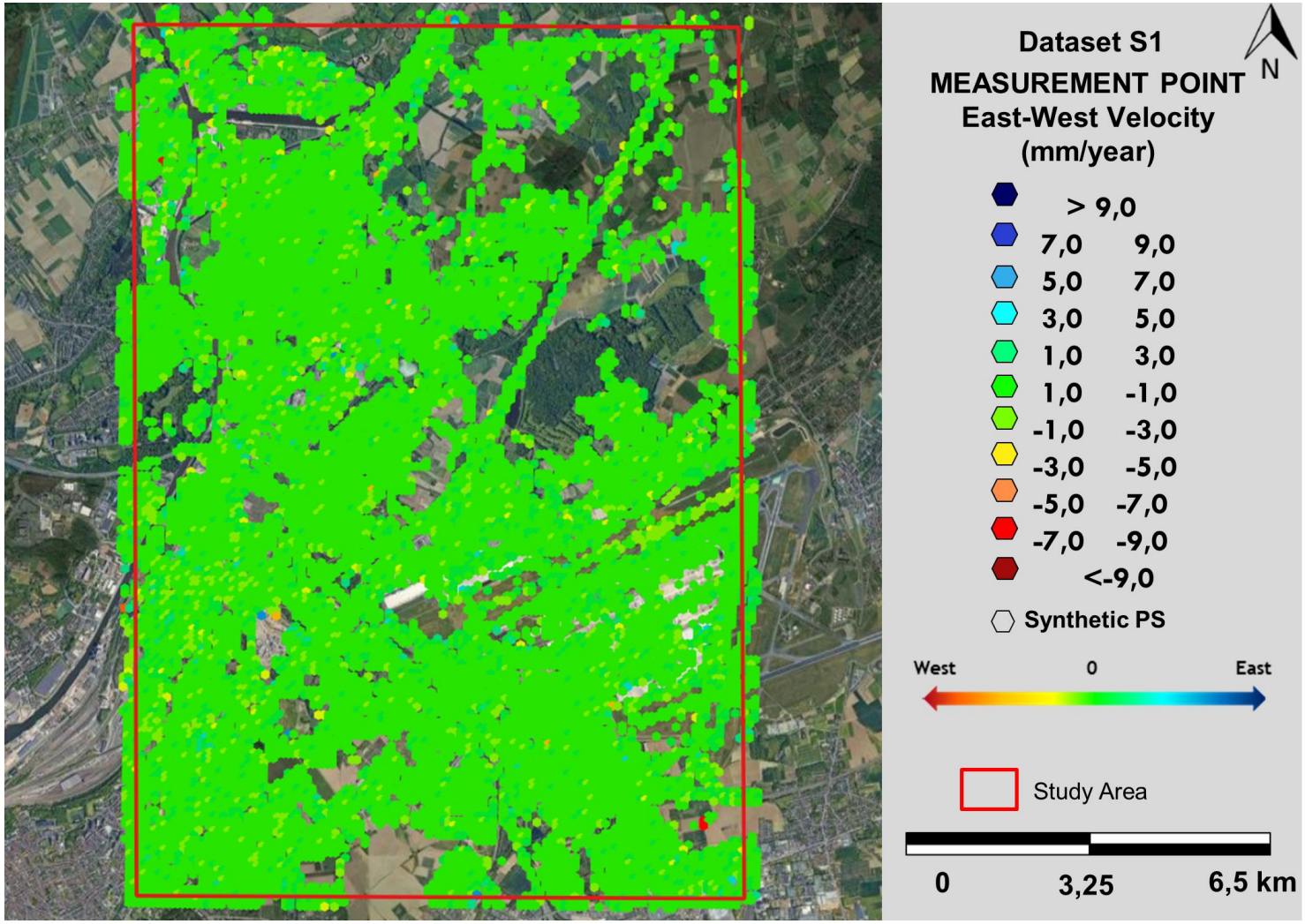


**Figure 9: The horizontal (East-West) component of the mean velocity obtained with the Sentinel-1 ascending and descending ground deformation measurements integration, relevant to the period March 2015 - July 2021. The obtained measurements are superimposed to an optical image.**

*NOT CLASSIFIED*
*This document discloses subject matter in which e-GEOS has proprietary rights. Recipient of the document shall not duplicate, use or disclose in whole or in part, information contained herein except for or on behalf of e-GEOS to fulfil the purpose for which the document was delivered to him.*

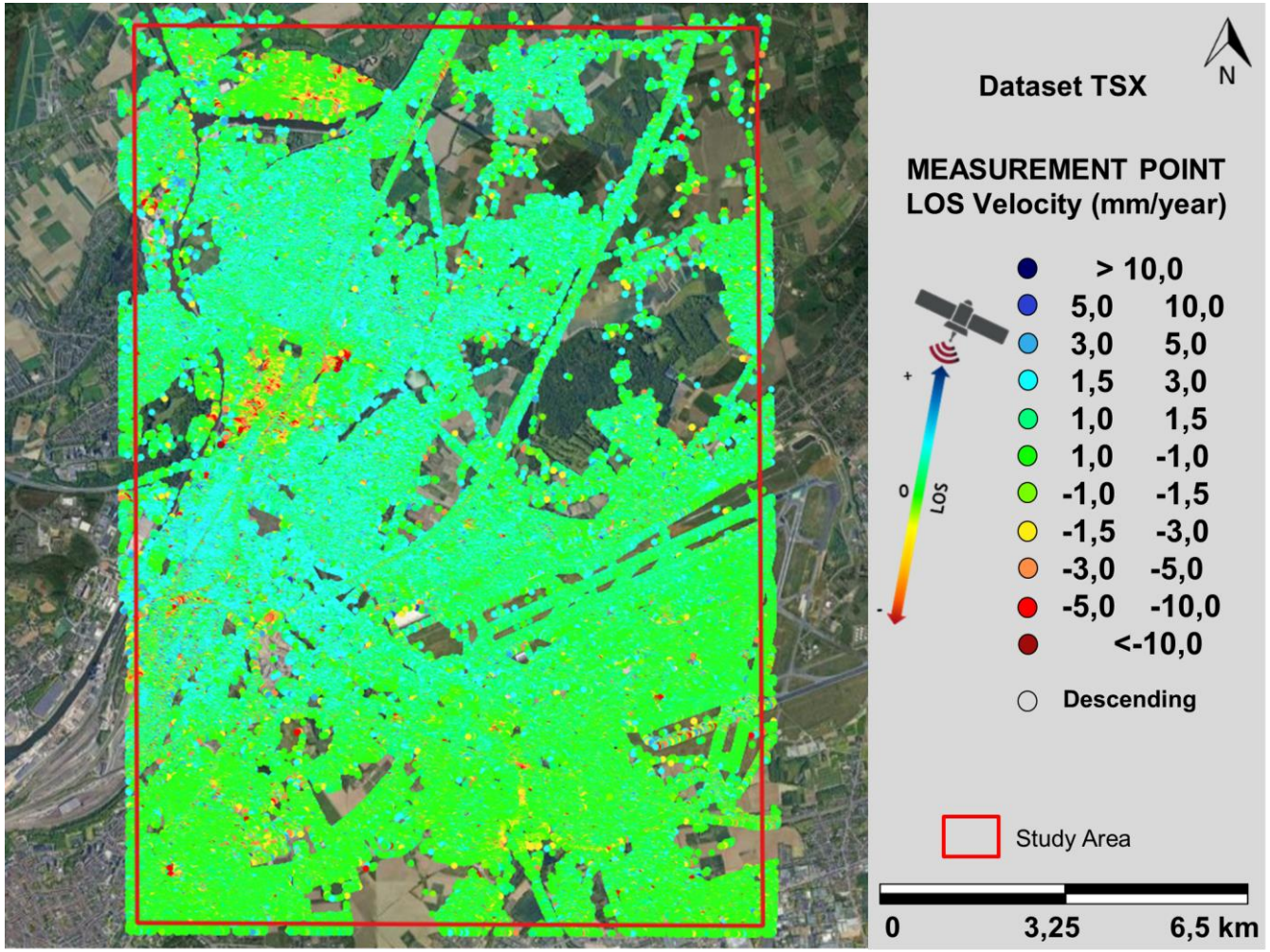


**Figure 10: The TerraSAR-X MP mean velocity map in descending geometry relevant to the period June 2014 - March 2016, obtained by the PSI technique. The stack is constituted by 53 TerraSAR-X Stripmap images, over Brussels, Belgium. The PS measurements are superimposed to an optical image.**

*NOT CLASSIFIED*
*This document discloses subject matter in which e-GEOS has proprietary rights. Recipient of the document shall not duplicate, use or disclose in whole or in part, information contained herein except for or on behalf of e-GEOS to fulfil the purpose for which the document was delivered to him.*

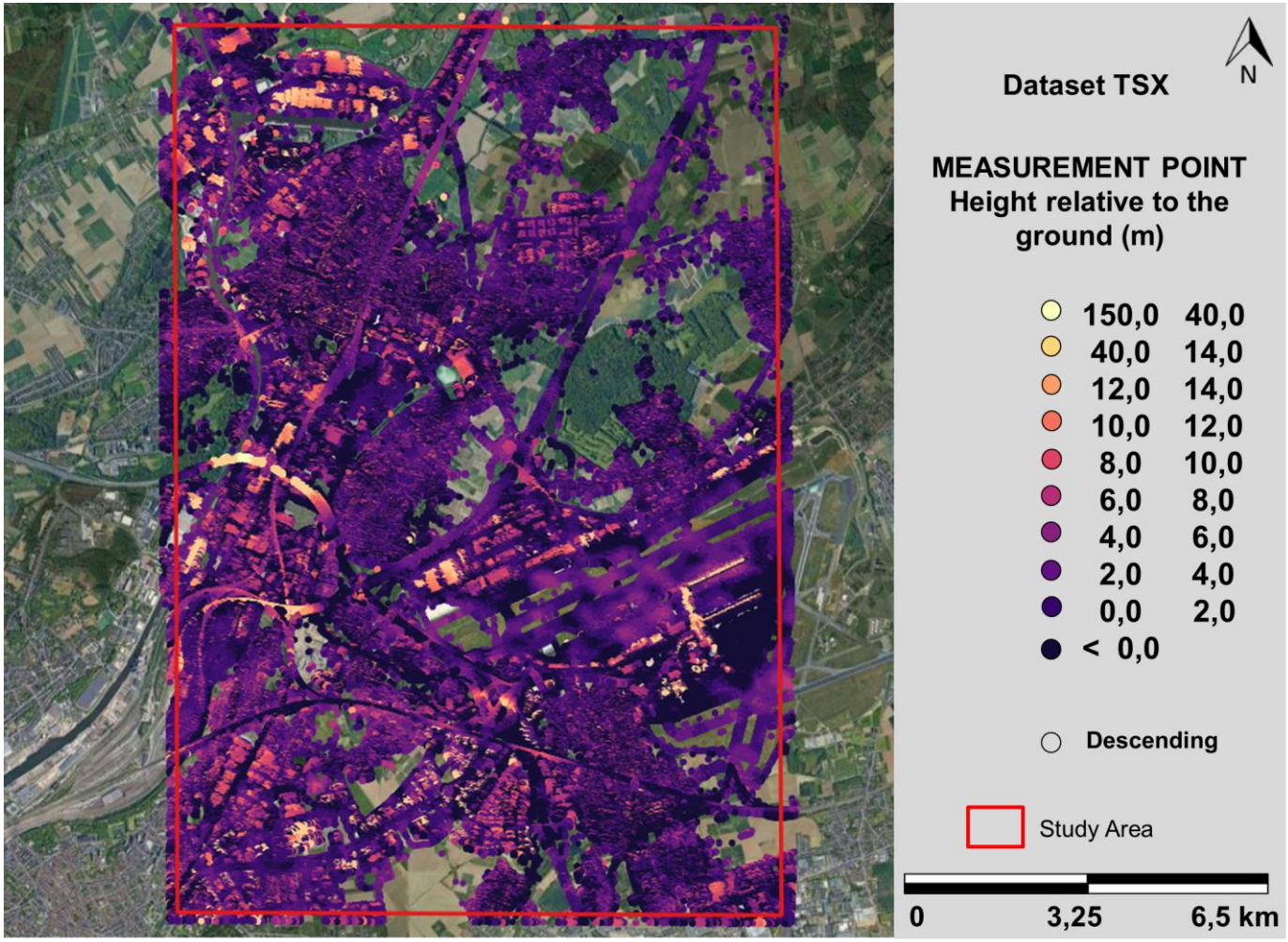


**Figure 11: The TerraSAR-X MP height relative to the ground (expressed in meters) map in descending geometry relevant to the period June 2014 - March 2016, obtained by the PSI technique. The stack is constituted by 53 TerraSAR-X Stripmap images, over Brussels, Belgium. The PS measurements are superimposed to an optical image**

*NOT CLASSIFIED*
*This document discloses subject matter in which e-GEOS has proprietary rights. Recipient of the document shall not duplicate, use or disclose in whole or in part, information contained herein except for or on behalf of e-GEOS to fulfil the purpose for which the document was delivered to him.*

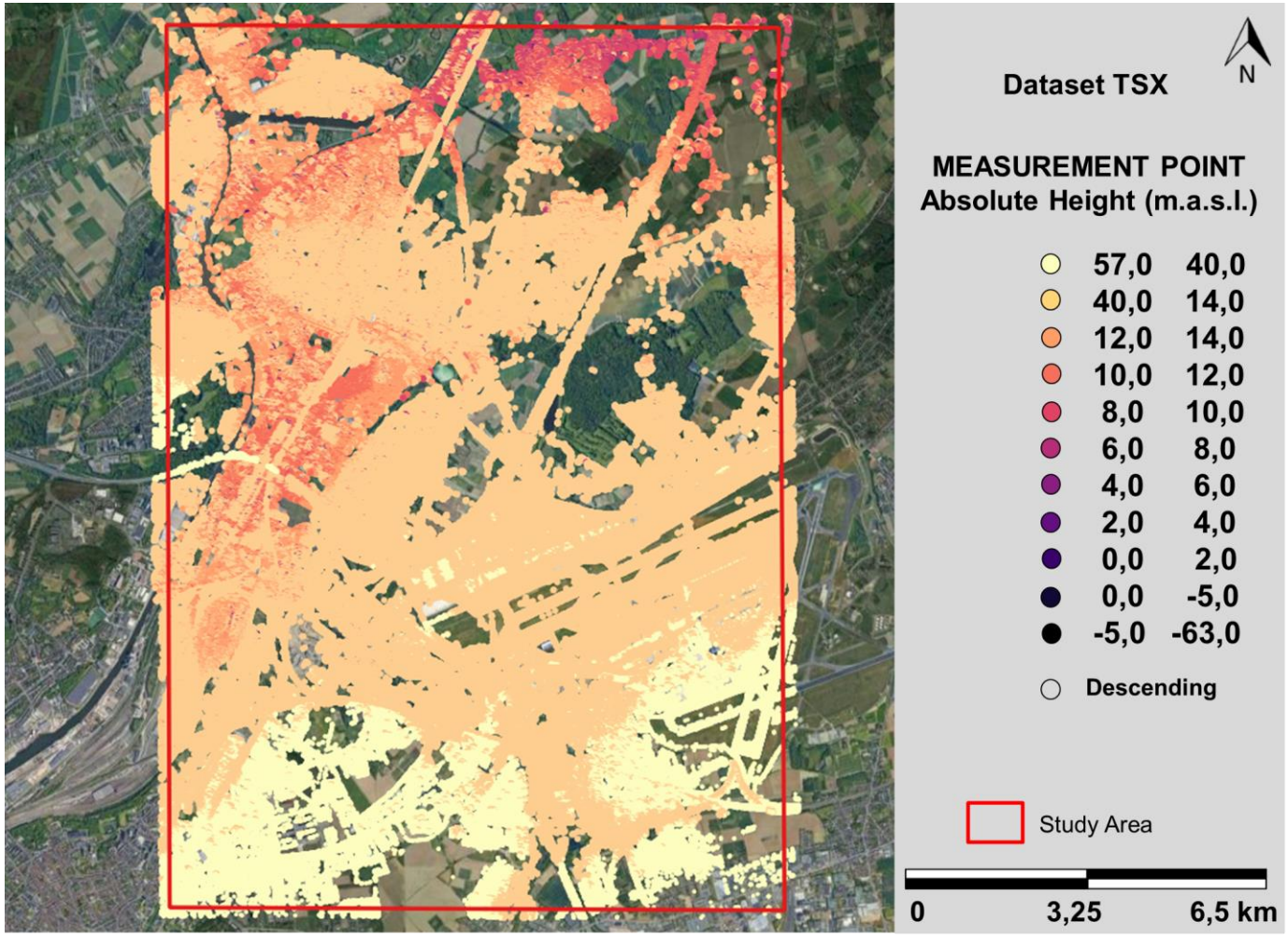


**Figure 12: The TerraSAR-X MP absolute height (expressed in meters a.s.l.) map in descending geometry relevant to the period June 2014 - March 2016, obtained by the PSI technique. The stack is constituted by 53 TerraSAR-X Stripmap images, over Brussels, Belgium. The PS measurements are superimposed to an optical image.**

*NOT CLASSIFIED*
*This document discloses subject matter in which e-GEOS has proprietary rights. Recipient of the document shall not duplicate, use or disclose in whole or in part, information contained herein except for or on behalf of e-GEOS to fulfil the purpose for which the document was delivered to him.*

# 8. Local analyses and interpretation of the results

The "InSAR Focus Analyses" allowed to perform detailed and site-specific analyses and control of measurement points. These analyses were performed for the bridges of interest and for specific limited areas affected by relevant and/or localized deformation processes detected during the InSAR Screening step.
The analyses were performed using proprietary software and tools organized in modular structures allowing a large flexibility to operate on the "raw" data, thus applying different methodologies according to the characteristics of the specific process under investigation among which: i) analysis module of amplitude and reflectivity data; ii) analysis of temporary scatterers (to further increase the sample of potential measurement points by exploiting newborn targets and/or coherent targets for specific time intervals); iii) analysis with different deformation models (e.g., non-linear); iv) localized area analyses, allowing to reduce the atmospheric noise for small-scale analysis.

***The technical sheets for each bridge of the PoC, with the main results of the performed post-processing and interpretation activity are showed in the Annex 1.***

Maximum availability of MP in case of works and filtering out of local disruptions have been successfully carried out thanks to information on maintenance works for each bridge provided by the Client.

| Object Nummer | Name | Information |
|---|---|---|
| 3186 | Havendoklaanbrug | no maintenance works |
| 5773 | Sluisstraatbrug | no maintenance works |
| 6135 | Verbrande Brug | new top layer (asphalt) in 2021 |
| 4463 | Hefbrug Vilvoordebrug Vuurkruisenlaan-Rubensstraat Europabrug | new top layer (asphalt) in 2015 |
| 4292 | Brug B14 | no maintenance works |
| 8042 | Viaduct in A201 over N262 | no maintenance works, pilars were treated between 2011 and 2013 |
| 4333 | Brug R18 | no maintenance works, pilars were treated between 2011 and 2013 |
| 4336 | Brug R21 | no maintenance works |
| 5843 | Viaduct R7 Deel B | right lane of inner ring, new top layer in 2021 |
| 5844 | Viaduct R7 Deel C | no maintenance works |
| 5845 | Viaduct R7 Deel D | no maintenance works |

*NOT CLASSIFIED*
*This document discloses subject matter in which e-GEOS has proprietary rights. Recipient of the document shall not duplicate, use or disclose in whole or in part, information contained herein except for or on behalf of e-GEOS to fulfil the purpose for which the document was delivered to him.*

| | | |
|---|---|---|
| 4317 | Viaduct R7 Deel A | no maintenance works |
| 3187 | Willemsbrug | renewing of bridge deck in 2016 - exact period not known |
| 8639 | Fiets- en voetbrug Schoewever Woluwelaan | no maintenance works |
| 9084 | Voet- en fietsbrug Kleine Steenstraat | no maintenance works |
| 8763 | Fietsbrug over E19 + Noordelijke spoorontsluiting luchthaven | no maintenance works |
| 8677 | Brug over de Zenne met verbindingsweg naar sluis | bridge was build/finalised in 2014-2015 |
| 9105 | Spoorwegbrug in Spoorlijn 25N over R22 | restoration from 01/08/2014-05/02/2015: additional anchoring of bridge deck in the abutments |
| 3189 | Tuchthuisbrug | no maintenance works |
| 4318 | Brug R8 P. Schoonstraat Oudstrijdersstraat | no maintenance works |
| 3590 | Brug 1 over de J. F. Kennedylaan Grensstraat | no maintenance works |
| 4323 | Brug R15 | new concrete new jerseys between bicycle lane and road, autumn 2014 |
| 4904 | Brug in N262 Parklaan over spoorweg | no maintenance works |
| 4332 | Brug D5 Steenweg op Zaventem | no maintenance works |

**Table 6: List of the bridges of the PoC and related information on maintenance works**

In particular, in order to obtain the maximum availability of MP in case of works and filtering out of local disruption, the ***Temporary Scatterers* (TS) *approach*** has been carried out. In fact, when targets do not have a stable backscatter radar signal along the all period of analysis, measurement points can be lost, as expected during works on bridges. In these cases, to maximize the number of MPs, different periods should be analyzed in correspondence of different bridges to avoid the use of SAR images when works are ongoing. This approach concludes with a puzzling of the different analyses covering different periods. This analysis can be performed automatically by exploiting the amplitude of the signal, thus analyzing separately the periods characterized by the same reflectivity behavior.

Furthermore, an **alerting system** procedure has been carried out allowing to distinguish among different 2 alert conditions: the *orange scenario*, when a first limit is exceeded (±3mm/yr); and the red scenario, when a second threshold is overcome (±5mm/yr).

The green color has been used where acceptable criteria for deformations are not exceeded, while white color when sufficient information to assess the condition is not available.

The alerting system can allow to consider both deformations related to the bridges and in the

*NOT CLASSIFIED*
*This document discloses subject matter in which e-GEOS has proprietary rights. Recipient of the document shall not duplicate, use or disclose in whole or in part, information contained herein except for or on behalf of e-GEOS to fulfil the purpose for which the document was delivered to him.*

surrounding area.

The final outputs of the activities are interference maps ( Figure 13, Figure 14 and technical sheets in Annex 1) reporting the geohazards and structural deformation processes and their degree of interference with the bridges.

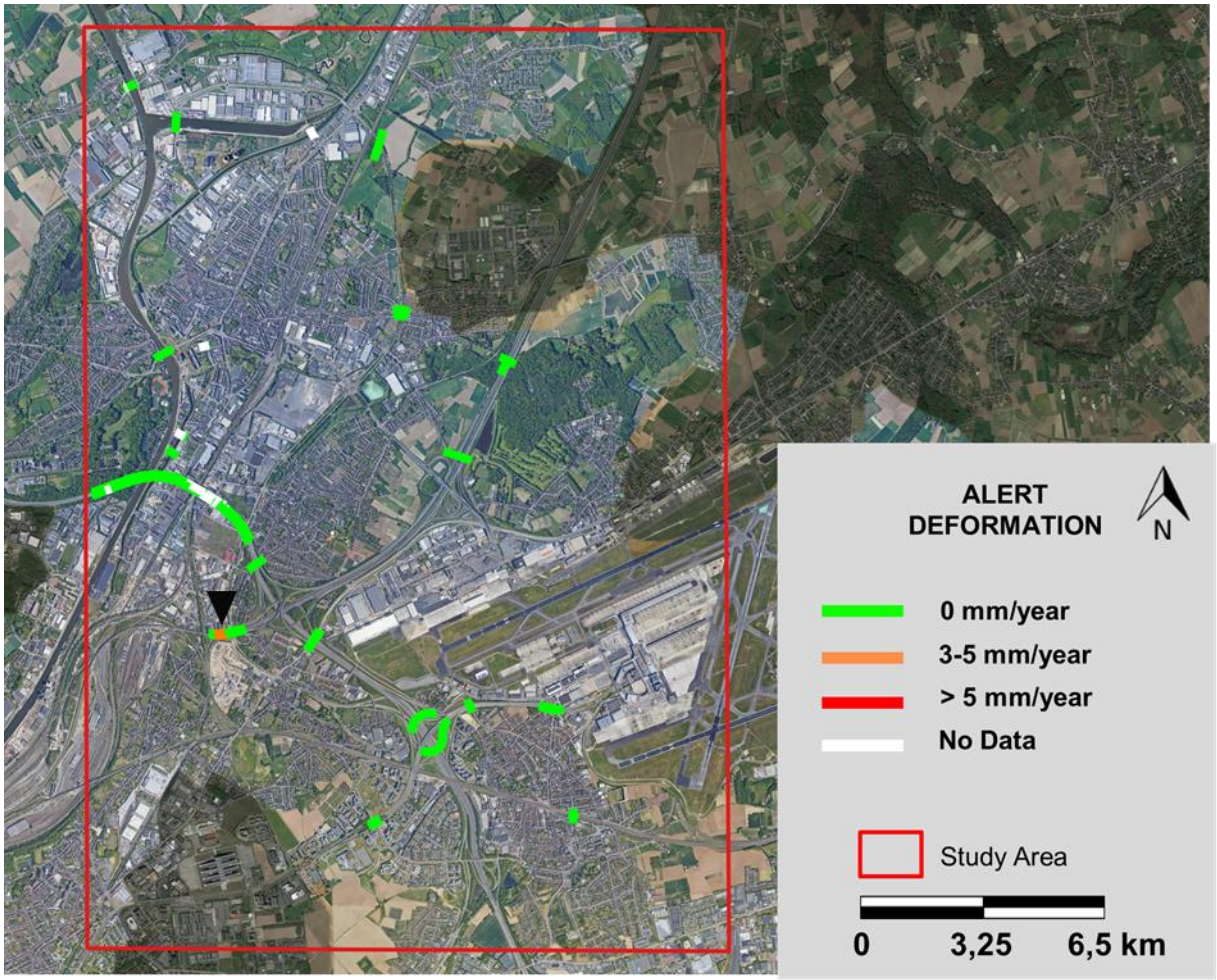


**Figure 13: Sentinel-1 interference map achieved by alerting system procedure. Orange color is when a first limit is exceeded (±3mm/yr); Red color is when a second threshold is overcome (±5mm/yr); The green color is used where acceptable criteria for deformations are not exceeded, while white color when sufficient information to assess the condition is not available.**

*NOT CLASSIFIED*
*This document discloses subject matter in which e-GEOS has proprietary rights. Recipient of the document shall not duplicate, use or disclose in whole or in part, information contained herein except for or on behalf of e-GEOS to fulfil the purpose for which the document was delivered to him.*

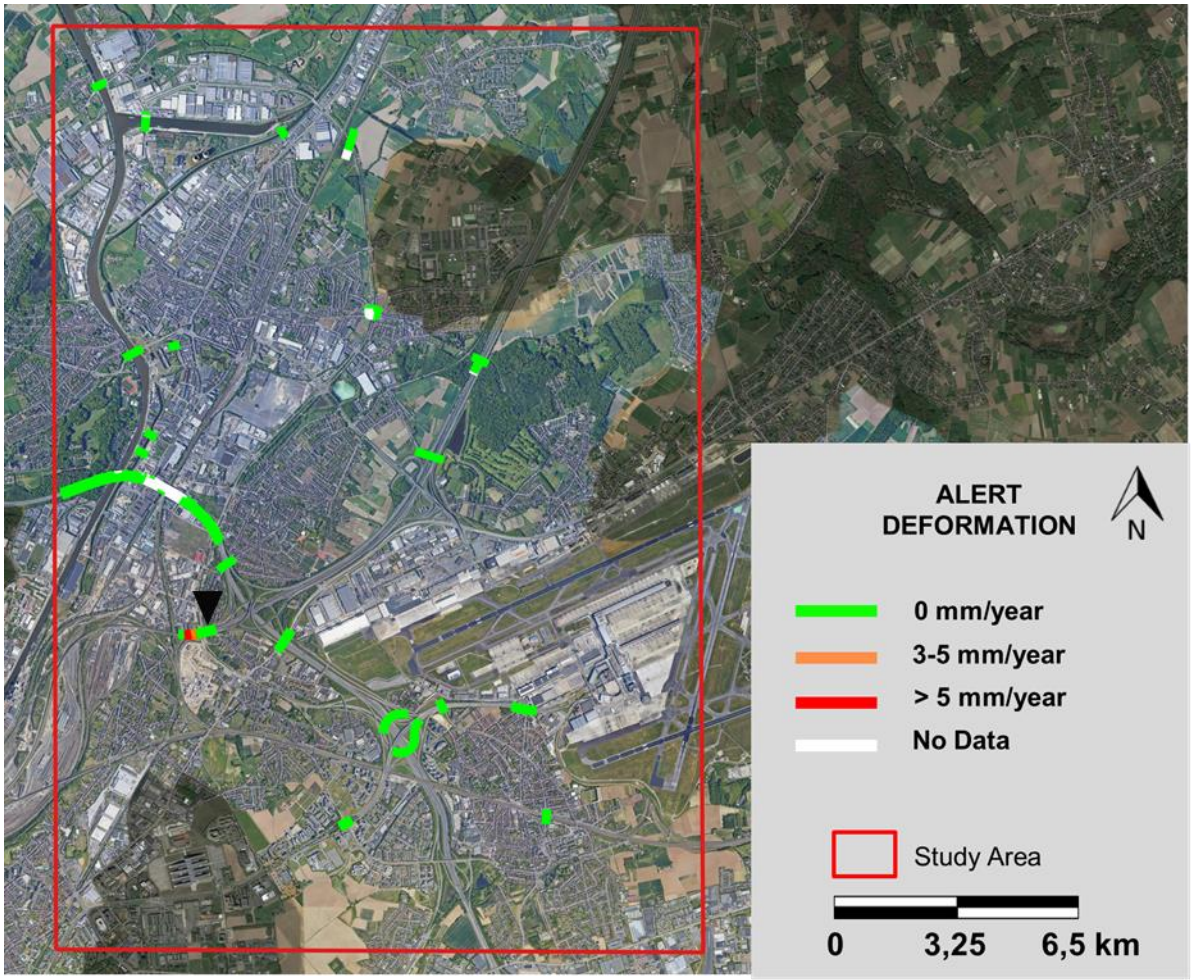


**Figure 14: TerraSAR-X interference map achieved by alerting system procedure. Orange color is when a first limit is exceeded (±3mm/yr); Red color is when a second threshold is overcome (±5mm/yr); The green color is used where acceptable criteria for deformations are not exceeded, while white color when sufficient information to assess the condition is not available.**

Lastly, during the PoC, we carried a 3D reconstruction of one bridge and its InSAR measurement points (Figure 15). It is worth mentioning that this has been possible according to the auxiliary data (engineering sections and 3D models acquired with photogrammetry or laser scanner or LIDAR) available. In particular, we used a detailed 3D model achieved from https://3dwarehouse.sketchup.com and modified by using 0.25cm LiDAR data to add InSAR results.

*NOT CLASSIFIED*
*This document discloses subject matter in which e-GEOS has proprietary rights. Recipient of the document shall not duplicate, use or disclose in whole or in part, information contained herein except for or on behalf of e-GEOS to fulfil the purpose for which the document was delivered to him.*

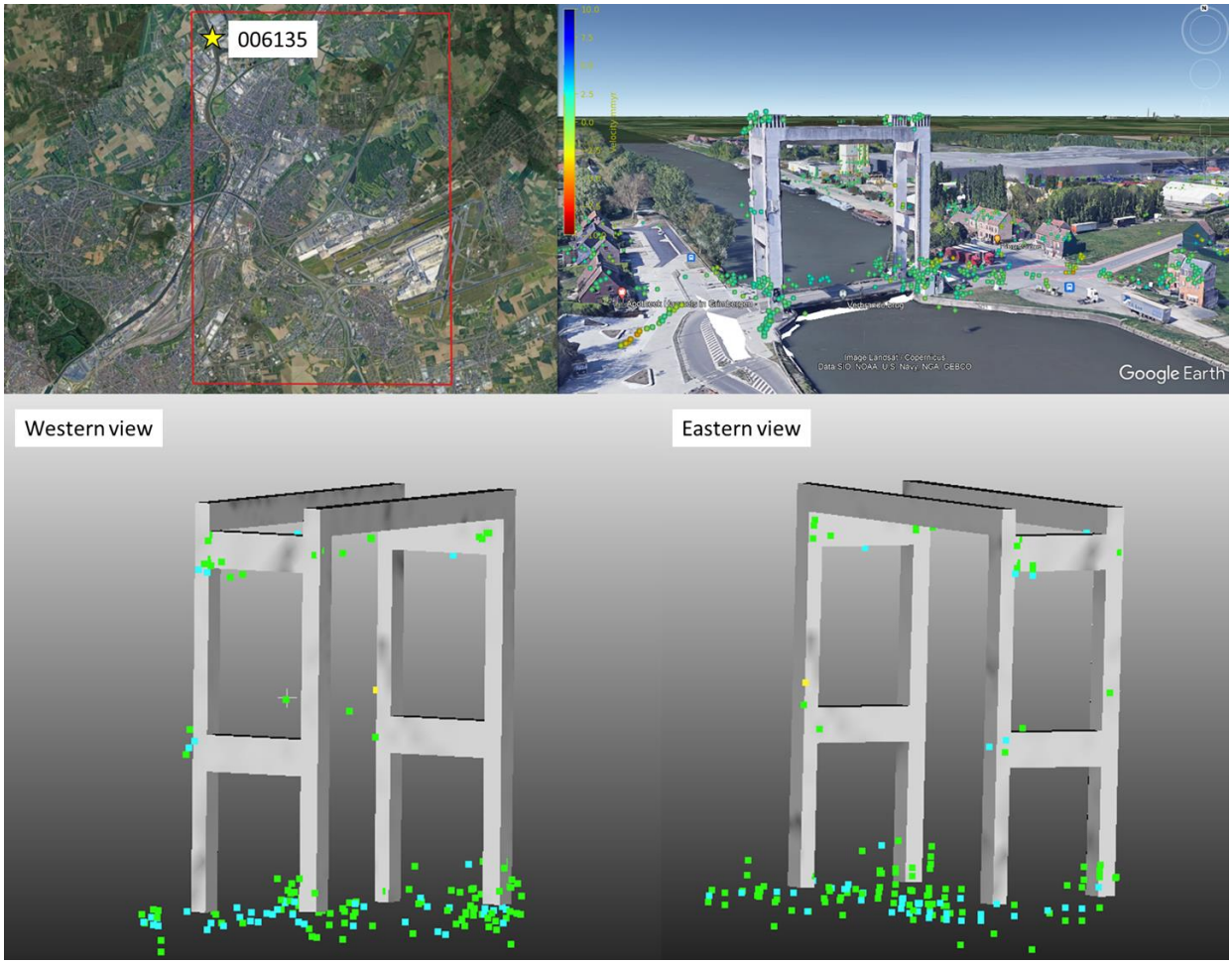


**Figure 15: 3D reconstruction of one bridge of the PoC (Verbrande Brug, 006135) with InSAR TerraSAR-X results view.**

## 9. Analysis and interpretation on lack of MPs

This section contains an analysis and interpretation of reasons on the lack of MPs observed in some portions of the Viaduct 47 (004317-005843-005844-005845).

The following Figure provides the area of interest of the PoC and location of the analysed bridges, in yellow the area of the Viaduct object of this analysis.

*NOT CLASSIFIED*
*This document discloses subject matter in which e-GEOS has proprietary rights. Recipient of the document shall not duplicate, use or disclose in whole or in part, information contained herein except for or on behalf of e-GEOS to fulfil the purpose for which the document was delivered to him.*

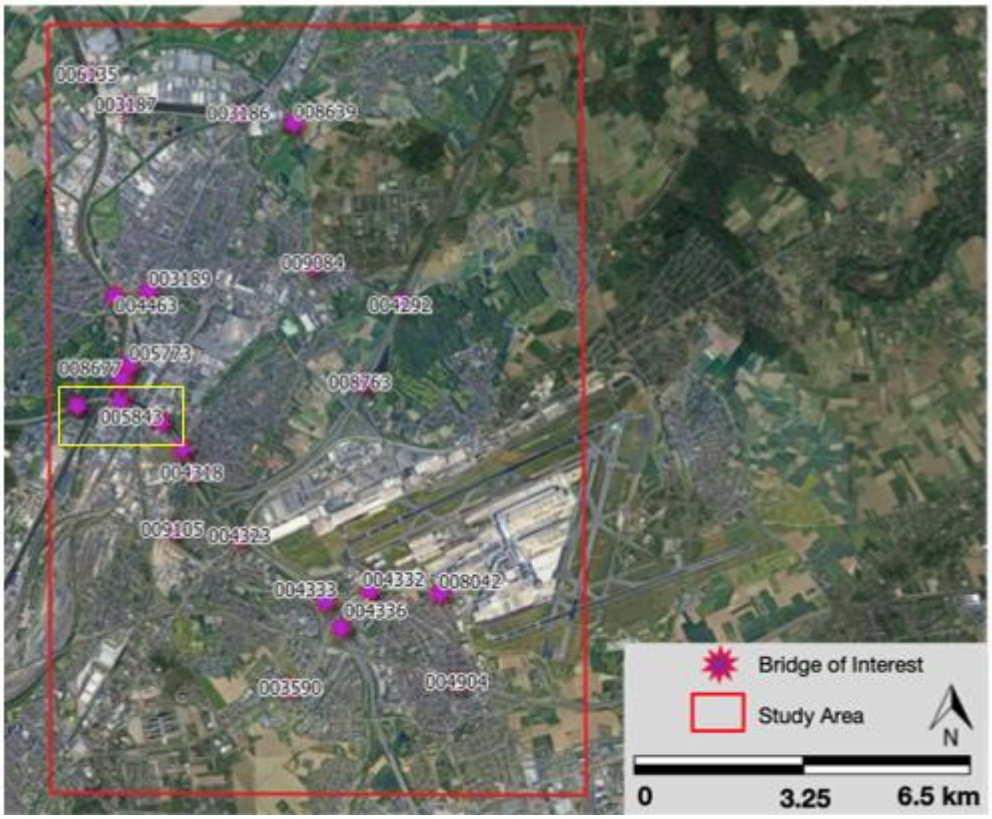


**Figure 16: Area of interest of the PoC and location of the bridges of interest provided by the client.**

As shown in Figure 17, with TerraSAR-X descending and Sentine-1 ascending/descending datasets, the portion of the structure lacking of MPs are highlighted by three ellipses.

In the ellipse n.1, a good number of MPs is present, but the density is lower than the surrounding areas. This is due to the presence of vegetation that affects the density of MPs achievable, introducing shadows and/or noise on the visibility of the structure, as demonstrated by the TerraSAR-X reflectivity map in Figure 19.

In the ellipse n.2, geometric distortions (Figure 18) are present, generated by the combination of topography and acquisition geometry (in the descending orbital geometry). On the contrary, the ascending orbital geometry is not affected by such geometric distortions in this sector, thanks to the different acquisition geometry with respect to the topography. This is the reason why Sentinel-1 ascending geometry allowed to achieve MPs on this sector.

In the ellipse n.3, the orientation of the structure is almost parallel to the TerraSAR-X and Sentinel-1 descending satellite LOS (Line of Sight) inducing a low visibility of this portion of the viaduct.

*NOT CLASSIFIED*
*This document discloses subject matter in which e-GEOS has proprietary rights. Recipient of the document shall not duplicate, use or disclose in whole or in part, information contained herein except for or on behalf of e-GEOS to fulfil the purpose for which the document was delivered to him.*

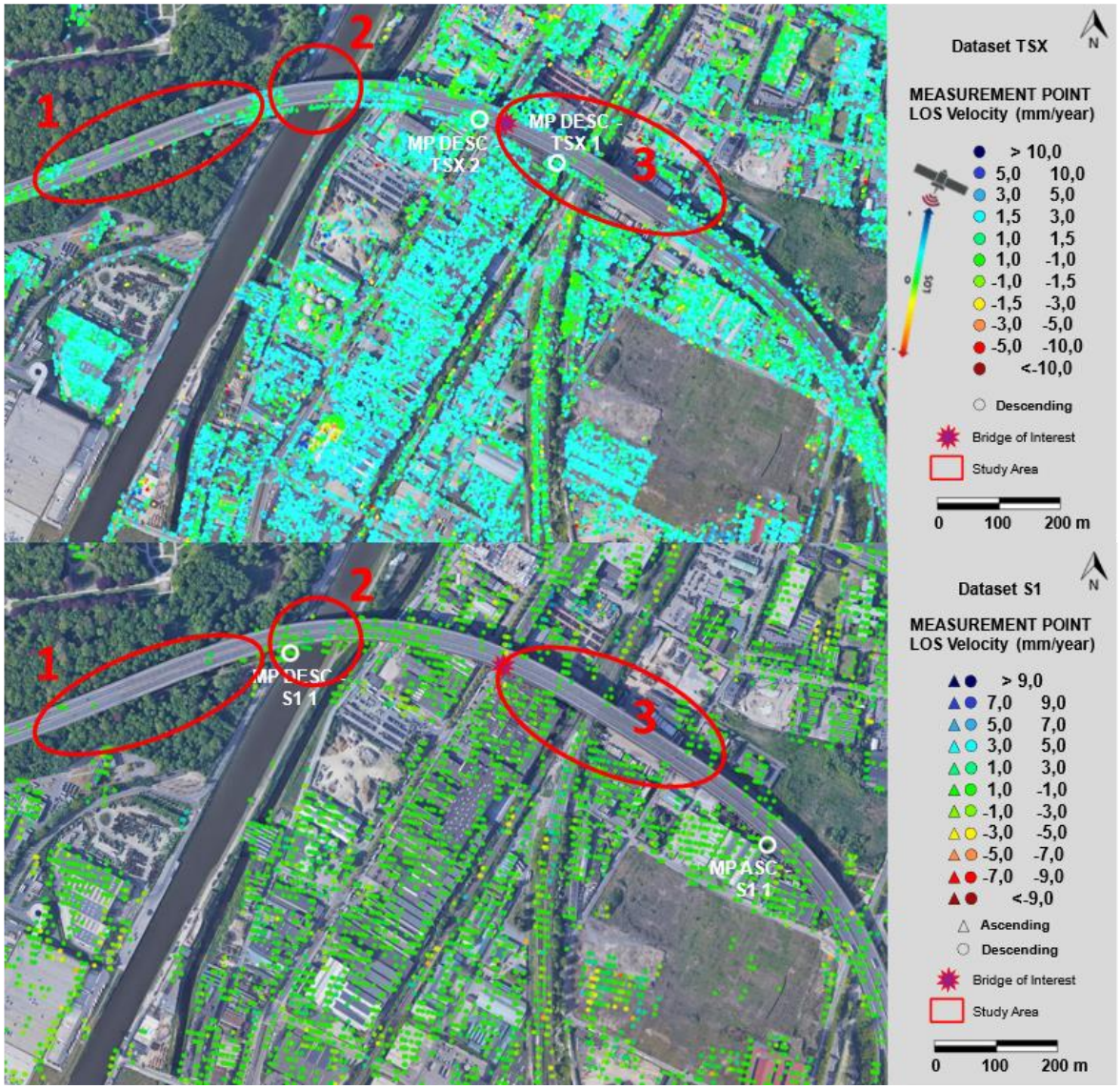


**Figure 17: The TerraSAR-X MP mean velocity map (top) in descending geometry and Sentinel-1 MP mean velocity map (bottom) in the ascending/descending geometries for the Viaduct 47. The ellipses represent portions of the structure with a lack or low density of MPs.**

*NOT CLASSIFIED*
*This document discloses subject matter in which e-GEOS has proprietary rights. Recipient of the document shall not duplicate, use or disclose in whole or in part, information contained herein except for or on behalf of e-GEOS to fulfil the purpose for which the document was delivered to him.*

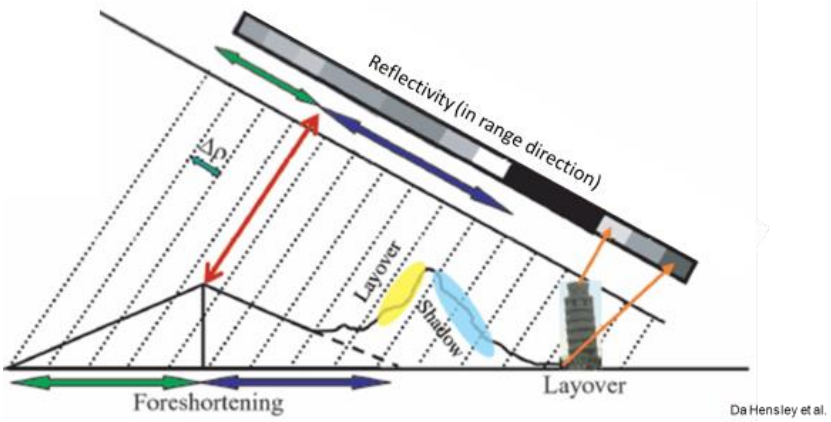


**Figure 18: main geometric distortions affecting SAR images (see Appendix).**

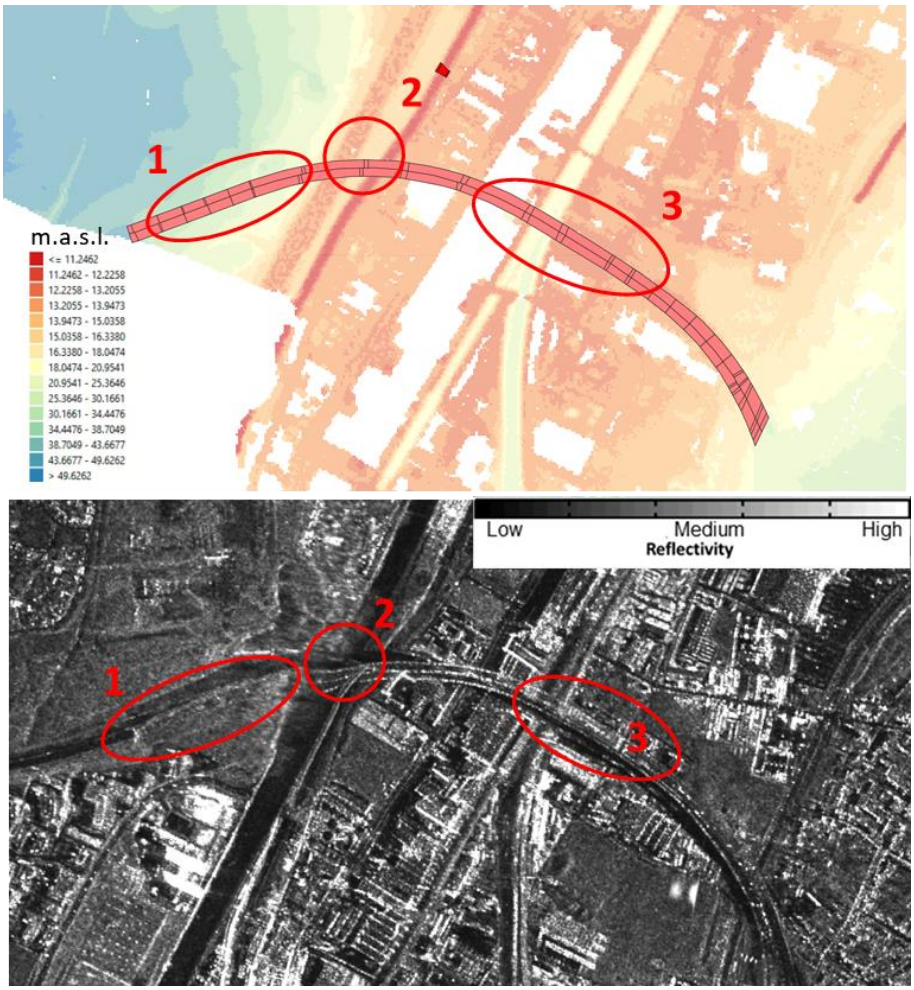


**Figure 19: 5m resolution digital elevation model (top) and TerraSAR-X Descending reflectivity map (bottom). In the ellipse n.1, the presence of vegetation affects the density of MPs achievable. In the ellipse n.2, geometric distortions of the images, generated by topography and acquisition geometry of the descending orbital geometry, are present. In the ellipse n.3, the orientation of the structure is parallel to the satellite descending LOS, inducing a low visibility of this portion of the viaduct.**

*NOT CLASSIFIED*
*This document discloses subject matter in which e-GEOS has proprietary rights. Recipient of the document shall not duplicate, use or disclose in whole or in part, information contained herein except for or on behalf of e-GEOS to fulfil the purpose for which the document was delivered to him.*

# 10. Conclusions

The analysis performed in the present POC and, especially, the results achieved by the post-processing analyses are a valuable support in achieving the objectives proposed for this tender procedure.

The A-DInSAR analyses have been performed using the available archive SAR images collected by the **Sentinel-1 satellite constellation (European Space Agency)**, acquired in **double geometry (ascending and descending)** in the period **February 2015 to August 2021**, for a total of 325 and 334 SAR images respectively, and the images acquired by **TerraSAR-X satellite constellation**, in **descending** acquisition geometry for the period **June 2014 to March 2016**, for a total of 53 high-resolution SAR images.

**A-DInSAR** technique has been applied in order to obtain information about past **long-term deformation** processes with **millimeter accuracy**, allowing to provide for each measurement point its trend of deformation along the LOS (in millimeters/year) and time series of displacement (in millimeters).

By the analysis of the **MPs velocity maps achieved by TerraSAR-X** (in descending orbital geometry), it can be highlighted that the area presents a portion subjected to uplift (ranging from +1 to +3 mm/yr). By literature resources and by the comparison with local morphology, this can be mainly linked to the groundwater recharge process currently active in the framework of the AOI. However, the rest of the study area presents little to no long-term deformations, by analyses with both Sentinel-1 and TerraSAR-X.

The complete coverage (100%) of the bridges has been achieved with high-resolution TerraSAR-X data. A good coverage (95%) of the bridges has been carried out with medium-resolution Sentinel-1 data: just one bridge (003186) is not covered by Sentinel-1, since the amplitude of the back scattering is very low in both geometries.

TerraSAR-X data allowed to estimate the height of each MP with high accuracy and allowing also to distinguish not only the MP belonging to the bridges, but also the different portions of each bridge, as we can see in the 3D plot of the MP in the technical sheets.

Both TerraSAR-X and Sentinel-1 allowed to well estimate and separate the long-term deformations and seasonal thermal oscillation of each bridge.

Temporary scatterers approach allowed to face and filtering out local disruptions or achieve MPs over bridges under construction.

The alerting system allowed to automatically highlight the portions of each bridge affected by relevant deformations.

*NOT CLASSIFIED*
*This document discloses subject matter in which e-GEOS has proprietary rights. Recipient of the document shall not duplicate, use or disclose in whole or in part, information contained herein except for or on behalf of e-GEOS to fulfil the purpose for which the document was delivered to him.*

For the execution of the POC, all the minimum and additional tender procedure requirements have been fulfilled. In particular, it is reported in the table below the section of the document of the corresponding requirement, with an overview of the adopted methodology.

| Requirement | | Where to find |
|---|---|---|
| **Minimum requirements** | | |
| 1 | Point-based deformation map | • Sect. 7, 8 and Annex 1 of the present report<br>• AWARE platform<br>• Geodatabases provided to the Client |
| 2 | PS and DS points | • AWARE platform<br>• Geodatabases provided to the Client |
| 3 | Platform | • AWARE manual<br>• AWARE platform |
| 4 | Display of deformation and deformation rate | • Sect. 7, 8 and Annex 1 of the present report<br>• AWARE platform<br>• Geodatabases provided to the Client |
| 5 | Distinction Sentinel - TerraSAR-X | • Sect. 7, 8 and Annex 1 of the present report<br>• AWARE platform<br>• Geodatabases provided to the Client |
| 6 | Accuracy | • Sect. 6 of the present report |
| 7 | Georeference | • Sect. 7, 8 and Annex 1 of the present report<br>• AWARE platform<br>• Geodatabases provided to the Client |
| 8 | Longitudinal and width profiles | • AWARE platform |
| 9 | Reporting | • The present report |
| **Additional requirements** | | |
| 10 | Maximum availability of results in case of works | • Sect. 8 and Annex 1 of the present report |
| 11 | Surroundings | • Sect. 7, 8 and Annex 1 of the present report<br>• AWARE platform<br>• Geodatabases provided to the Client |
| 12 | Automation of analysis | • Sect. 5 and 8 of the present report |

*NOT CLASSIFIED*
*This document discloses subject matter in which e-GEOS has proprietary rights. Recipient of the document shall not duplicate, use or disclose in whole or in part, information contained herein except for or on behalf of e-GEOS to fulfil the purpose for which the document was delivered to him.*

| | | |
|---|---|---|
| 13 | Filtering out of local disruptions | • Sect. 8 and Annex 1 of the present report |
| 14 | Automation of longitudinal profiles | • Sect. 8 and Annex 1 of the present report<br>• AWARE platform |
| 15 | Detection of sudden changes in displacement | • Sect. 8 of the present report<br>• AWARE platform |
| 16 | Temperature variations | • Sect. 7, 8 and Annex 1 of the present report<br>• AWARE platform<br>• Geodatabases provided to the Client |
| 17 | Alerting system | • Sect. 8 and Annex 1 of the present report<br>• AWARE platform |
| 18 | Reliability of results per bridge | • N/A in the bridges of present PoC, but the procedure is implemented and ready to be used |
| 19 | Horizontal displacement | • Sect. 7, 8 and Annex 1 of the present report<br>• AWARE platform<br>• Geodatabases provided to the Client |
| 20 | In-depth analysis of zones where no InSAR points are available | • Sect. 7, 8, 9 and Annex 1 of the present report<br>• Additional note to the technical report provided on 24 Dec 2021 |

**Table 7: Traceability matrix for the Tender Requirements**

While the Sentinel-1 images present a ground resolution of 4m × 14m, the TerraSAR-X sensor ground resolution is 3m x 3m. Through the meticulous assessment and comparison of Sentinel-1 and TerraSAR-X satellite results for each single structure of interest, it has been possible to identify the main differences between the two sensors and define some key points.

By using TerraSAR-X satellite data it has been possible to determine MPs over all the bridges of the POC, with a clear distinction between points belonging to the infrastructure with respect to the other elements. On the contrary, by using Sentinel-1 it was not possible to define MPs over every single bridge of interest.

As regards Minimum requirement #8 and Additional requirement #14, the automation of longitudinal profile is currently available using the specific AWARE Tool *Deformation Cross Section* and *Deformation Profile*, by drawing a line with a buffer, to which require the automatic processing of profile. If the Tender requirement means to provide the automatic

*NOT CLASSIFIED*
*This document discloses subject matter in which e-GEOS has proprietary rights. Recipient of the document shall not duplicate, use or disclose in whole or in part, information contained herein except for or on behalf of e-GEOS to fulfil the purpose for which the document was delivered to him.*

provision of the profile for some bridges at the same time, It will be foresee, during the implementation phase, a development to automate this operation, given a set of predefined segments, in correspondence of each bridge of interest.

As regards Additional requirement #16, the Temperature variations is currently available in AWARE including both the Velocity (VEL) and the Velocity without thermal component (VEL_NO_TE), and both can be visualized separately using the specific AWARE Tool *Palette Selection*, by selecting the parameter VELOCITY or VELOCITY WITHOUT TH.EXPANCION.

Notwithstanding it was not requested in the Tender, as regards Additional requirement #16, additional databases has been provided containing the long-term time series of displacement of each MP cleaned from the thermal component, respectively for Sentinel-1 and TerraSAR-X datasets. This shapefile has been added to allow the analysis of the evolution of the VEL_NO_TE.

The results provide a demonstration that the added value of the InSAR analysis can be a precious mean to monitor the deformations of bridges.

Additionally, it is also possible to determine the convenience of the high-resolution images when performing such kind of analyses for linear infrastructures as bridges. With high resolution data, all the bridges have been covered by the InSAR analysis, due to a higher amount and higher density of MPs. This allows to better distinguish points belonging to the infrastructure with respect to the other elements. The geolocation accuracy of the MPs obtained through the high-resolution data is greater than the one corresponding to the medium resolution data.

***NOT CLASSIFIED***
***This document discloses subject matter in which e-GEOS has proprietary rights. Recipient of the document shall not duplicate, use or disclose in whole or in part, information contained herein except for or on behalf of e-GEOS to fulfil the purpose for which the document was delivered to him.***

# APPENDIX: General introduction on InSAR service

## Satellite SAR Interferometry

InSAR (*Interferometric Synthetic Aperture Radar*) (Massonnet et al., 1998; Hanssen, 2001) can be considered one of the most powerful satellite remote sensing techniques used for the measurement of displacements of the Earth's surface. It is based on the comparison between RADAR images acquired in different times over the same area. The basic principle of Multi-Image InSAR or Advanced DInSAR methodologies (A-DInSAR) consists of the combination of information from a large number of SAR images, allowing to derive the temporal evolution of displacements of objects on the ground during the period of analysis.

A-DInSAR techniques allow to detect deformation processes, both past (historical analysis) and/or in progress, and to estimate their evolution in time and space.

## General information on SAR (Synthetic Aperture Radar) systems

RADAR (***Radio Detection And Ranging***) are systems able to emit an electromagnetic pulse in the domain of microwaves and to register the return signal (**echoes**) backscattered by the objects in the instrumental field of view (**targets**). For this reason, RADAR systems are considered **active** remote sensing systems, since they don't need an external source of energy (like solar lighting), but they make use of energy (pulse) generated by the sensor. So, for example, they are able to "*see*" through clouds (in case of satellite or aerial based radar platforms).

By RADAR systems, it is possible to detect objects and to measure their distances from the sensor. For this reason, the backscattering characteristics of the targets in the field of view are very important, as well as their **dielectric** properties.
**SAR (*Synthetic Aperture Radar*)** is a specific kind of RADAR system: the main characteristic of SAR systems is to take advantage of the motion of the sensor along a pre-defined trajectory (e.g., the orbit of a satellite equipped with the SAR sensor) in order to observe the same area from different points of view, thus simulating a large antenna able to get high resolution on the ground. This specific geometry of acquisition is sketched in Figure 20.

*NOT CLASSIFIED*
*This document discloses subject matter in which e-GEOS has proprietary rights. Recipient of the document shall not duplicate, use or disclose in whole or in part, information contained herein except for or on behalf of e-GEOS to fulfil the purpose for which the document was delivered to him.*

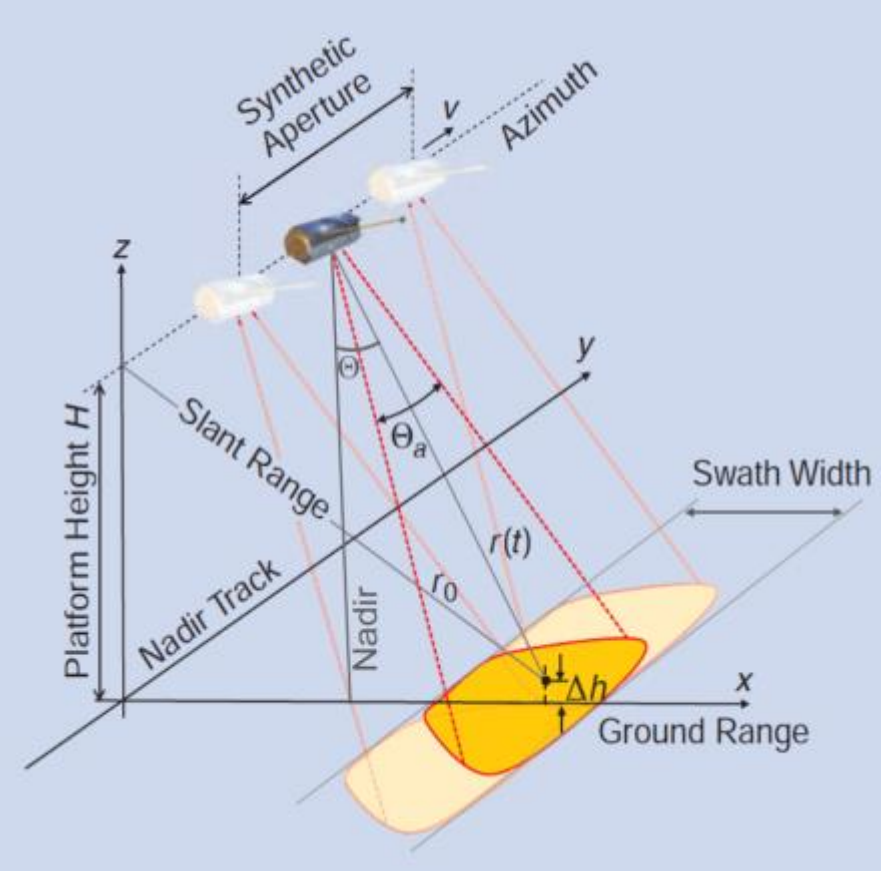


**Figure 20: SAR acquisition geometry.**

SAR images are characterized by a ***Slant Range*** and ***Azimuth*** resolution. The first one (*Slant Range*) refers to the resolution along the direction of propagation of the RADAR signal, orthogonal to the satellite orbit, which is inclined with an *off-nadir* angle θ specific for each satellite. The second one (*Azimuth*) refers to the resolution along the flight direction that, in case of satellite, corresponds to the orbit that can be approximately considered North-South.

*NOT CLASSIFIED*
*This document discloses subject matter in which e-GEOS has proprietary rights. Recipient of the document shall not duplicate, use or disclose in whole or in part, information contained herein except for or on behalf of e-GEOS to fulfil the purpose for which the document was delivered to him.*

### SAR satellite images

A satellite SAR image is made up by a matrix of pixels arranged along the directions of azimuth (parallel to the movement of the satellite) and slant range (orthogonal with respect to the flight direction).

Each pixel contains information about amplitude and phase of the signal backscattered from the observed objects. Amplitude represents the energy of the signal reflected to the sensor, while the phase contains the most important information for interferometric purposes: the distance between the sensor and the backscattering target on the ground.
Satellites can collect data into two different orbital geometries: the satellite revisits the same area following both a path approximately from North to South (descending geometry) and a path from South to North (ascending geometry) (Figure 21). So, the same area is detected by two different angles of view.

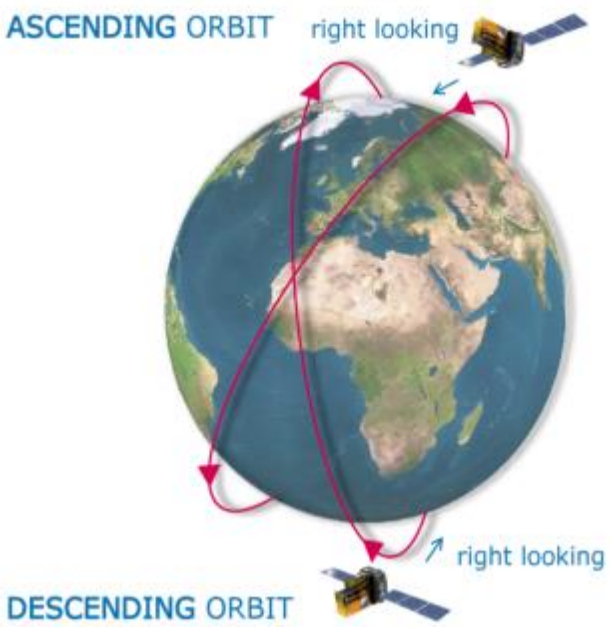


**Figure 21: acquisition geometries of SAR images.**

The acquisition geometry, according to the orbits of the SAR sensors, can introduce some uncertainties in the detection of deformation processes characterized by some specific features. For example, areas characterized by steep slopes may appear distorted (i.e. *foreshortening* effect) or even be in shadow (*shadowing*). In these cases, the analysis of the data can be complex and inaccurate (Figure 22).
Moreover, movements with a strong N-S horizontal component cannot be properly analyzed and the displacement values can be underestimated.

*NOT CLASSIFIED*
*This document discloses subject matter in which e-GEOS has proprietary rights. Recipient of the document shall not duplicate, use or disclose in whole or in part, information contained herein except for or on behalf of e-GEOS to fulfil the purpose for which the document was delivered to him.*

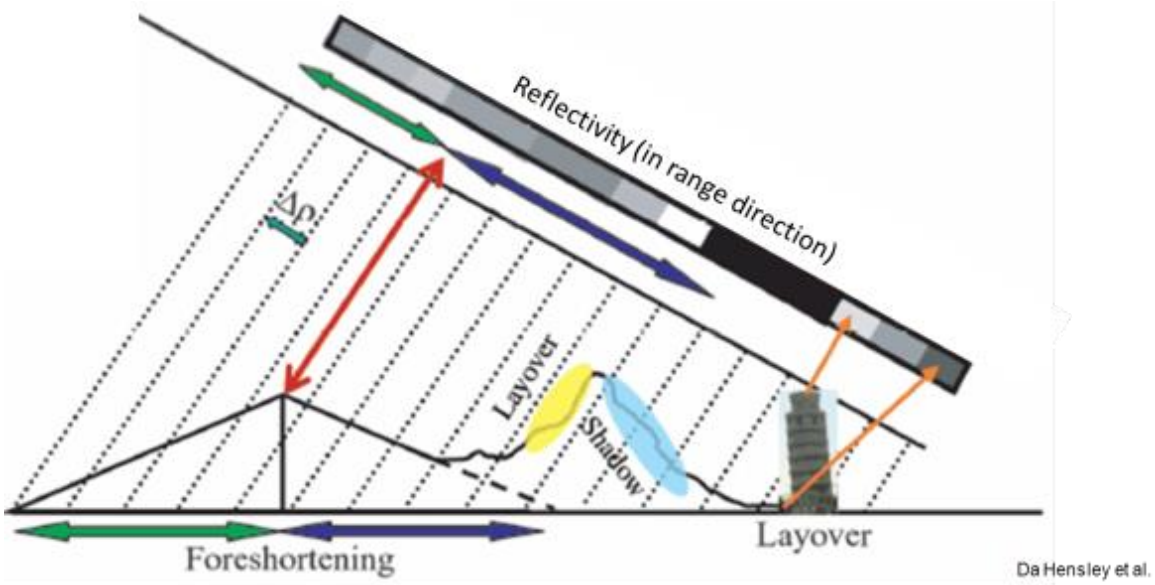


**Figure 22: main geometric distortions.**

**Basic Principles of differential SAR interferometry (DInSAR)**

DInSAR (Differential Interferometric SAR) is the traditional technique used for the detection of displacements from SAR Interferometry. It is based on the analysis of the variation of the phase signal between pairs of images collected at different times over the same area, thus allowing to measure the displacements on the Earth's surface.

Information about the phase difference is derived from the **Interferogram** which represents the basic element of this methodology.

In particular, the phase of each pixel is the sum of two terms:

$$\boxed{\varphi = \varphi_s + \varphi_r} \quad (1)$$

The first ($\varphi_s$) is related to the scatterers within the scene; the second ($\varphi_r$) depends on the double path satellite-target and on the wavelength of the electromagnetic pulse emitted and then recorded by the sensor:

$$\boxed{\varphi_r = \frac{4 \cdot \pi \cdot r}{\lambda}} \quad (2)$$

*NOT CLASSIFIED*
*This document discloses subject matter in which e-GEOS has proprietary rights. Recipient of the document shall not duplicate, use or disclose in whole or in part, information contained herein except for or on behalf of e-GEOS to fulfil the purpose for which the document was delivered to him.*

*r* is the distance between the satellite and the target on the ground along the range direction and $\lambda$ is the wavelength. However, the phase of a single SAR image cannot be used because:

• $\varphi_s$ is random;

• $\varphi_r$ depends on *r*, that is in the order of hundreds of kilometers, and on λ that, on the contrary, is in the order of few centimeters.

In fact, the electromagnetic wave, for each pixel, is sent from the SAR antenna to the Earth's surface; during the satellite-ground path, the sinusoidal signal performs millions of cycles, hits the targets with a particular phase value and it's randomly backscattered (multiple reflections, $\varphi_s$ ). Finally, part of the signal returns to the satellite, that records the information.

By considering the phase difference between two SAR images, $\varphi_s$ of the same target is deleted and the **interferometric phase** $\Delta\phi$ is given by:

$$\boxed{\Delta\phi = \frac{4 \cdot \pi}{\lambda} \cdot \Delta R} \quad (3)$$

$\Delta\phi$ is characterized by the following main contributions:

$$\boxed{\Delta\phi = \Delta\phi_f + \Delta\phi_{topo} + \Delta\phi_{displ} + \Delta\phi_{atm} + \Delta\phi_{err}} (4)$$

$\Delta\phi_f$ is called "flat earth phase" and is due to the different angles of view of the satellites during the acquisition of the image. It is a contribution easy to remove.

$\Delta\phi_{topo}$ is the phase component containing the topographical information, that is the relation between phase and height. This phase contribution can be estimated by using a *DEM* (Digital Elevation Model).

$\Delta\phi_{atm}$ represents a random element caused by the different weather conditions during the acquisition of SAR images over time.

*NOT CLASSIFIED*
*This document discloses subject matter in which e-GEOS has proprietary rights. Recipient of the document shall not duplicate, use or disclose in whole or in part, information contained herein except for or on behalf of e-GEOS to fulfil the purpose for which the document was delivered to him.*

$\Delta\phi_{displ}$ is the contribution to the interferometric phase due to the earth's surface displacements.
$\Delta\phi_{err}$ is a residual noise, not directly calculable.

The differential interferogram is obtained from (4). The flat earth contribution and the topographic phase can be easily removed using a DEM. So, to detect the displacement information, $\Delta\phi_{atm}$ and $\Delta\phi_{err}$ must be estimated. The acquisition system of the interferometric pairs of SAR images is characterized by the geometric baseline (also called normal or perpendicular baseline) (Figure 23) and by the temporal baseline (i.e. the time interval between two consecutive acquisitions), which can influence the quality of the results obtained by the DInSAR analysis. The normal baseline is related to the different orbital positions of the satellite during the acquisition of SAR images on the same area over time. Orbits, in fact, can slightly deviate respect to the nominal trajectory (in the order of some hundreds of meters) and the same area is looked at with slightly different angles.
The temporal baseline, on the other hand, introduces artifacts known as “temporal decorrelation” which becomes more and more remarkable with the increasing of the time elapsed between the acquisition of two subsequent SAR images. Such degradation of the quality is due to the variation of conditions like changes in vegetation cover, frosts, thaws, building works etc.

The interpretation of interferometric data can be further complicated due to changes of the weather conditions during the two acquisitions. The atmospheric artifacts (also known as “*Atmospheric Phase Screen*”) are among the main limitations for these techniques; that is the reason why many interferograms are necessary in order to estimate and remove it.

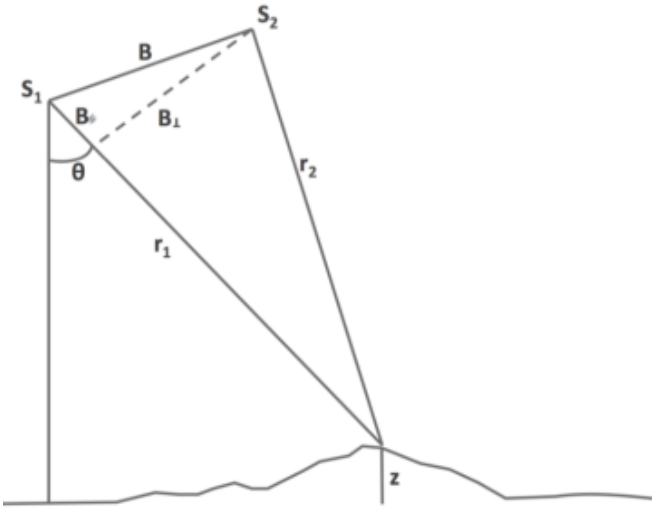


**Figure 23: geometric baseline. Acquisition geometry of two SAR images. S1 and S2 represent the position of the satellites at different times; *θ* is the nadir-off angle; $r_1$ and $r_2$ are the satellite-target distances for two acquisitions; *B* schematically represents the geometric baseline; *z* is the measured topographic height.**

*NOT CLASSIFIED*
*This document discloses subject matter in which e-GEOS has proprietary rights. Recipient of the document shall not duplicate, use or disclose in whole or in part, information contained herein except for or on behalf of e-GEOS to fulfil the purpose for which the document was delivered to him.*

**Advanced DInSAR (A-DInSAR)**

The development of interferometric multi-image techniques (or Advanced DInSAR) represented a significant step forward in the analysis of Earth's surface deformation using satellite SAR images. The use of datasets made of many SAR images allows the estimation and the removal of the atmospheric contribution. By such methodologies, the multi-temporal analysis of deformation processes can be performed, and time series of displacement can be estimated for a very large number of measurement points (MP) on the observed scene.

A-DInSAR techniques are based on the analysis of objects characterized by strong stability over time in terms of reflectivity. So, these objects are favored "**measurement points**", having specific properties allowing to perform accurate measurements of displacement (in the order of a few millimeters). Good reflectors are, for example: buildings, transportation routes (roads, railways), pylons, dams, bridges etc. Under specific conditions, also outcropping rocks are good reflectors. This dense *natural* network of "measurement points" allows to detect both local-scale deformation processes (e.g., those affecting a single building or structure) and large-scale deformation processes (e.g., landslides, subsidence, faults, etc.).

It is worth noting that the displacement of the measurement points is detected **along the instrumental line of sight (LOS)**. This implies that the measured displacement is the projection of the real displacement vector along the **sensor-target line**. For vertical movements (e.g., subsidence), the actual displacement can be easily retrieved by basic trigonometric functions; if the target is affected also by horizontal displacements, the achieved measurement is the result of the projection of all the components on the LOS. Using SAR images collected by different orbital geometries (ascending and descending) it is possible to perform more complex post-processing analysis to estimate the horizontal and the vertical components of the actual displacement vector.

Moreover, the measurements of velocity are also differential: they do not express an absolute value of displacement over time, but a relative displacement with respect to a reference point, i.e., a point within the investigated area that is assumed as stable (not affected by movement).

Each measurement point is characterized by a **temporal coherence** value, that is a measure of the fitting between the measured data and the deformational model used in the analysis.

If the characteristics of the backscattering targets change over time, the interferometric phase will contain a random noise that will affect the reliability of the results, causing a decrease of the temporal coherence. Interferometric coherence ranges between 0 (no correlation between corresponding pixels of the two SAR images) to 1 (full correlation).

Thanks to A-DInSAR techniques we can retrieve for each measurement point:

- the position (i.e., its geographic coordinates: latitude and longitude);

*NOT CLASSIFIED*
*This document discloses subject matter in which e-GEOS has proprietary rights. Recipient of the document shall not duplicate, use or disclose in whole or in part, information contained herein except for or on behalf of e-GEOS to fulfil the purpose for which the document was delivered to him.*

- the average velocity of displacement (along the line sensor-target, LOS) in mm/year, with an accuracy depending on the number of available images and the sensor used (up to a few millimeters);
- the time series of displacement, starting from the first available image, with an accuracy of few millimeters on the single measure for the most reliable measurement points.

The main advantages introduced by A-DInSAR techniques are:

- the measurement points generate a "natural geodetic network": they, in fact, are already on the ground, such as buildings, roads, railways, anthropic elements, outcropping rocks. For each of them (if archive images are available) it is possible to obtain displacement measurements since 1992;
- the aerial extension of SAR images makes it possible to analyze large areas in a short time;
- the measuring accuracy is very high, thus allowing the detection of slow phenomena over large areas otherwise not detectable;
- the achieved results can be easily imported and visualized into geographic information systems (GIS) allowing rapid integration with other available data;
- the dual acquisition geometry (ascending and descending) improves the quality of the information about the analyzed phenomenon: in fact, by decomposing the velocity vectors and combining the two geometries, it is possible to retrieve the displacement vector component on the horizontal plane (E-W) and on the vertical axis. The horizontal component along the N-S direction cannot be measured because the orbits of operating satellites follow approximately meridian orbits.

Finally, concerning A-DInSAR techniques it is worth noting that:

- the presence of good targets as well as a suitable density of measurement points are required. For example, in areas completely vegetated or not visible from the satellite (e.g., shadowing), it is not possible to get information. On the other hand, densely urbanized areas are usually characterized by a very big number of measurement points, allowing to perform accurate analyses;
- the analysis of deformation processes characterized by quick evolution is quite difficult to be performed by A-DInSAR techniques and, in some cases, only qualitative information can be retrieved by a priori assumptions. Moreover, often impulsive phenomena cannot be monitored by this technique, especially when centimeter-scale displacements occur in a short time and in extremely localized areas.

*NOT CLASSIFIED*
*This document discloses subject matter in which e-GEOS has proprietary rights. Recipient of the document shall not duplicate, use or disclose in whole or in part, information contained herein except for or on behalf of e-GEOS to fulfil the purpose for which the document was delivered to him.*

# Reference documents

Declercq, P.Y., Pirard, E. and Devleeschouwer, X., 2012. BRUSSELS: 20 YEARS OF UPLIFTING MONITORED BY RADAR INTERFEROMETRY (PSI). 7thEUREGEO, p.484.

Declercq, P.Y., Walstra, J., Gérard, P., Pirard, E., Perissin, D., Meyvis, B. and Devleeschouwer, X., 2017. A Study of Ground Movements in Brussels (Belgium) Monitored by Persistent Scatterer Interferometry over a 25-Year Period. Geosciences, 7(4), p.115.

Choopani, Atefe, Pierre-Yves Declercq, Alain Dassargues, and Xavier Devleeschouwer. "Land Subsidence Observed in the Merchtem Area (Flanders)–30 Years of SAR Data Associated to Groundwater Withdrawal?." In 2021 IEEE International Geoscience and Remote Sensing Symposium IGARSS, pp. 8392-8395. IEEE, 2021.

M. Costantini, S. Falco, F. Malvarosa, F. Minati, A new method for identification and analysis of persistent scatterers in series of SAR images, Proceedings of the IEEE International Geoscience and Remote Sensing Symposium (IGARSS '08), Boston, Ma, USA, 6-11 06/2008.

M. Costantini, S. Falco, F. Malvarosa, F. Minati and F. Trillo, Method of persistent scatterer pairs (PSP) and high resolution SAR interferometry, Proceedings of the IEEE International Geoscience and Remote Sensing Symposium (IGARSS '09), Cape Town, South Africa, 07/2009.

M. Costantini, S. Falco, F. Malvarosa, F. Minati, F. Trillo, F. Vecchioli, Persistent Scatterer Pairs (PSP) Approach in Very High Resolution SAR Interferometry, EUSAR 2010 - 8th European Conference on Synthetic Aperture Radar, 7-10 06/2010.

M. Costantini, F. Malvarosa, F, Minati, A General Formulation for Redundant Integration of Finite Differences and Phase Unwrapping on a Sparse Multidimensional Domain, IEEE Transactions on Geoscience and Remote Sensing, vol. 50, no. 3, pp. 758-768, doi 10.1109/TGRS.2011.2162630, 2012.

M. Costantini, F. Malvarosa, F. Minati, and F. Vecchioli, Multiscale and block decomposition methods for finite difference integration and phase unwrapping of very large datasets in high resolution SAR interferometry, Proceedings of the IEEE International Geoscience and Remote Sensing Symposium (IGARSS '12), Munich, Germany, 07/2012, pp. 5574-5577.

Hanssen, Ramon F. (2001), “Radar Interferometry: Data Interpretation and Error Analysis”, Kluwer Academic, ISBN 9780792369455.

Massonnet, D.; Feigl, K. L. (1998), "Radar interferometry and its application to changes in the earth’s surface", Rev. Geophys.36(4): 441–500,: 1998 RvGeo. 36.441M.

*NOT CLASSIFIED*
*This document discloses subject matter in which e-GEOS has proprietary rights. Recipient of the document shall not duplicate, use or disclose in whole or in part, information contained herein except for or on behalf of e-GEOS to fulfil the purpose for which the document was delivered to him.*